DEVELOPMENT OF A DROSOPHILA CMT4A MODEL USING IMAGO APPROACH

by

Kerem Yıldırım

B.S., Molecular Biology and Genetics, Boğaziçi University, 2011

Submitted to the Institute for Graduate Studies in
Science and Engineering in partial fulfillment of
the requirements for the degree of
Master of Science

Graduate Program in Molecular Biology and Genetics

Boğaziçi University

2013

to my family…

ACKNOWLEDGEMENTS

First of all, I would like to express my sincere thanks to my thesis supervisor Prof. Esra Battaloglu for her great supervision, guidance and encouragement during this study. It has been a great pleasure to work in her laboratory.

I also would like to thank my co-advisor Assoc. Prof. Arzu Çelik for her guidance, valuable discussions and support in the course of this study. I am very grateful to her for investing so much time and effort into this project.

I owe my special thanks to Prof. Kuyaş Buğra Bilge, Assoc. Prof. Nesrin Özören and Prof. Arzu Karabay Korkmaz for devoting their valuable time to evaluate my thesis.

I would also like to express my special thanks to my colleagues Kaya, Merve K., Burçak, Merve S., Duygu D., Begüm, Cansu, Büşra and Alperen. They've been more than friends to me. I wish to thank the members of Lab 204; Aslı, Neslihan, Mahmut Can, Balkan, Burcu, Emirhan, Harun, and Yıldız; and also the Fly lab members; Gamze, Ece, Bahar, Stefan, Selen, and Güner.

My very specific thanks go to Duygu Koldere, who was always there for me. Through her encouragement and constant support, together with her endless patience, I was able to overcome many difficulties.

I would like to extend my gratitude to my aunt, who has been always with me.

Last but not least, I would like to thank my family for their unconditional love and support throughout my life.

Finally, I am grateful to TUBITAK-BIDEB 2210 for awarding and financially supporting me during my studies towards a master degree. This project is funded by TUBITAK, project number 112T275.

ABSTRACT

DEVELOPMENT OF A DROSOPHILA CMT4A MODEL USING IMAGO APPROACH

Charcot-Marie-Tooth (CMT) disease is the most common inherited peripheral neuropathy. So far, approximately 50 genes and loci have been associated with CMT. Mutations in ganglioside-induced differentiation-associated protein 1 (GDAP1), cause demyelinating, axonal, or intermediate subtypes of CMT with recessive or dominant segregation. GDAP1 is involved in mitochondrial network dynamics and oxidative stress mechanisms in which perturbations lead to neurodegenerative diseases. However, the molecular mechanisms causing CMT pathogenesis are not clearly understood. GDAP1 is a conserved protein in Eukarya and *CG4623* is the *Drosophila* homolog of GDAP1 with 49% similarity and 31% identity at the amino acid level. The aim of this study is to develop a *Drosophila* model for CMT disease by silencing the *CG4623* gene. In the first part of the project, *CG4623* was down-regulated spatiotemporally using the RNA interference (RNAi) method. Ubiquitous down-regulation of *CG4623* levels resulted in a significant decrease in the mRNA levels by more than 80% compared to control flies. Tissue-specific down-regulation of *CG4623* in glia revealed defects in mitochondrial dynamics in peripheral nerves of larvae. However, this observation could not be verified using the available image analysis and quantification software. In the second part of the project, a fly line that harbors a targeting construct for knocking out *CG4623* was generated using an integrase-mediated approach for gene knockout (IMAGO). The target vector was injected to *Drosophila* embryos with the expectation of site-specific integration into the second chromosome. This line was crossed with SceI & Flp lines and the progeny was screened for *CG4623* knockout flies. During these crosses it was observed that the construct was integrated into the X chromosome instead of the second. This integration was unexpected; however it does not affect future crosses and analyses. More progeny flies should be screened in order to obtain *CG4623* knockout flies.

ÖZET

İAGSY YAKLAŞIMINI KULLANARAK BİR CMT4A DROSOPHILA MODELİNİN GELİŞTİRİLMESİ

Charcot-Marie-Tooth (CMT) en sık görülen kalıtsal periferal nöropatidir. Şimdiye kadar CMT ile ilişkilendirilen 50 gen ve kromozom bölgesi bulunmaktadır. Ganglioside-induced differentiation-associated protein 1 (*GDAP1*) bu genlerden biridir ve mutasyonları, çekinik veya baskın kalıtım gösterebilmekte ve demiyelizan, aksonal, veya ara CMT alttiplerine neden olmaktadır. GDAP1'ın mitokondriyal ağ dinamikleri ve oksidatif stres yolaklarında rol aldığı ve bu yolaklardaki bozuklukların nörodejeneratif hastalıklara neden olduğu bilinmektedir. Ancak CMT patogenezine neden olan moleküler mekanizmalar henüz net olarak çözümlenememiştir. GDAP1 ökaryotlar arasında evrimsel olarak korunmuş bir proteindir ve *Drosophila* homoloğu *CG4623*'tür. Bu iki protein aminoasit düzeyinde %31 aynı, %49 benzerlik göstermektedir. Bu çalışmanın amacı *CG4623* genini susturarak, CMT hastalığı için *Drosophila* modeli oluşturmaktır. Projenin ilk aşamasında, RNA interferans (RNAi) metodu ile *CG4623* anlatımı istenilen dokularda baskılanmıştır. *CG4623*'ün anlatımı tüm dokularda baskılandığında mRNA seviyesi, kontrollere kıyasla %80 azalmıştır. Baskılama deneyleri glia-spesifik gerçekleştirildiğinde larval periferal sinir demetlerinde mitokondri dinamiğinde farklılık gözlenmiştir. Fakat gözlenen farklılıklar görüntüleme ve nicelik analizleri ile doğrulanamamıştır. Projenin ikinci aşamasında, *CG4623*'ün genomdan integraz aracılığı ile silinmesi yöntemi (IAGSY) kullanılmıştır. Geni hedefleyen plasmid yapısı hazırlanmıştır ve hedef plazmid bölgeye özel integrasyon ile ikinci kromozom hedeflenerek *Drosophila* embriyolarına mikroenjeksiyon yöntemi ile aktarılmıştır. Elde edilen sinek hattı SceI/Flp sinek hatları ile çaprazlanmakta ve *CG4623* silinmiş sinekler kırmızı göz markörü yardımı ile taranmaktadır. Tarama sırasında hedef yapının ikinci kromozom yerine X kromozomuna entegre olduğu belirlenmiştir. Ender görülen bu durumun ileri aşamalarda gerçekleştirilmesi beklenen analizleri gölgeleyecek bir etkisi bulunmamaktadır. *CG4623*'ün silindiği sinek hatlarını elde etmek için daha fazla sayıda çaprazlama ve tarama gerçekleştirilmelidir.

TABLE OF CONTENTS

LIST OF FIGURES

LIST OF TABLES

LIST OF SYMBOLS

kDa	Kilodalton
m	Meter
mg	Milligram
ml	Milliliter
mM	Millimolar
v	Volume
w	Weight
µg	Microgram
µl	Microliter
µm	Micrometer

LIST OF ACRONYMS / ABBREVIATIONS

AD	Autosomal Dominant
attP	Attachment Site P
attB	Attachment Site B
BAC	Bacterial Artificial Chromosome
bp	Basepair
BSA	Bovine Serum Albumin
Ca	Calcium
CaCl2	Calcium Chloride
cDNA	Complementary Deoxyribonucleic Acid
CMAP	Compound Muscle Action Potential
CMT	Charcot-Marie-Tooth
CMT1	Charcot-Marie-Tooth Type 1
CMT2	Charcot-Marie-Tooth Type 2
CMT4A	Charcot-Marie-Tooth Type 4A
CT	Comperative Threshold Cycle
ddH_2O	Double Distilled Water
DNA	Deoxyribonucleic Acid
Drp1	Dynamin-related Protein 1
EDTA	Ethylenediamine Tetraacetate
Elav	Embryonic Lethal, Abnormal Vision
Fis1	Fission 1
Flp	Flippase
FRT	Flippase Recognition Target
GCT	Guanidium Thiocyanate
GDAP1	Ganglioside-induced Differentiation-associated-Protein 1
GDAP1L1	Ganglioside-induced Differentiation-associated Protein 1 Like 1
GFP	Green Fluorescent Protein
GST	Glutathione S-transferase
GTP	Guanosine Triphosphate

GTC	Guanidium Thiocyanate
H_2O	Water
HA	Homology Arm
HCl	Hydrochloric Acid
HD	Hydrophobic Domain
HMSN	Hereditary Motor and Sensory Neuropathy
IMAGO	Integrase-mediated Approach for Gene Knockout
kb	Kilobase
KCl	Potassium Chloride
LB	Luriana Bertani
Mb	Megabase
MCS	Multiple Cloning Site
Mff	Mitochondrial Fission Factor
Mfn1	Mitofusin 1
Mfn2	Mitofusin 2
MgCl2	Magnesium Chloride
$MgSO_4$	Magnesium Sulfide
MiD49	Mitochondrial Dynamic Protein of 49 Kilodalton
MiD51	Mitochondrial Dynamic Protein of 51 Kilodalton
min	Minute
ml	Milliliter
mM	Millimolar
MNCV	Motor Nerve Conduction Velocity
MOM	Mitochondrial Outer Membrane
MOPS	3-(N-morpholino) Propane Sulfonic Acid
MSC	Myelinating Schwann Cells
NaCl	Sodium Chloride
NaOH	Sodium Hydroxide
NGS	Normal Goat Serum
NMJ	Neuromuscular Junction
NMSC	Nonmyelinating Schwann Cells
Opa1	Optic Atrophy Protein 1
PBS	Phosphate Buffered Saline

PCR	Polymerase Chain Reaction
PFA	Paraformaldehyde
PMP22	Peripheral Myelin Protein 22
PNS	Peripheral Nervous System
PR	Photoreceptor Cells
qRT-PCR	Quantitative Real Time Polymerase Chain Reaction
RbCl	Rubidium Chloride
Repo	Reversed Polarity
RMCE	Recombinase-mediated Cassette Exchange
RNA	Ribonucleic Acid
RNAi	Ribonucleic Acid Interference
ROS	Reactive Oxygen Species
SCP	Schwann Cell Precursors
shRNA	Short Hair-pin Ribonucleic Acid
siRNA	Small Interfering Ribonucleic Acid
TA	Tail-anchored
TAE	Tris-Acetate-EDTA
TFB1	Transformation Buffer 1
TFB2	Transformation Buffer 2
TMD	Transmembrane Domain
TUBB	Tubulin Beta Class I
UAS	Upstream Activating Sequence
UV	Ultraviolet
VDRC	Vienna *Drosophila* Resource Center
VNC	Ventral Nerve Cord

1. INTRODUCTION

1.1. Mammalian Peripheral Nervous System

Mammalian nervous system is a complex network that provides communication within and outside the body. It is subdivided into central (CNS) and peripheral nervous system (PNS) and each part is built out of neurons and supporting glial cells. Internal and external inputs are carried within the neurons as electrochemical signals and processed into outputs such as walking or shaking hands. Glial cells are not only protecting neurons, but also supporting them by supplying oxygen and nutrients. Astrocytes and oligodendrocytes are the main glial cells in the CNS, while Schwann cells and satellite cells are the two types of glial cells found in the PNS (Bhatheja and Jeffrey, 2006; Jessen, 2004).

In PNS development, neural crest cells give rise to Schwann cell precursors (SCP) and subsequently to immature Schwann cells. Afterwards, immature Schwann cells differentiate into either myelinating (MSC) or non-myelinating (NMSC) Schwann cells (Jessen, 2004). NMSCs are required for survival and maintenance of axons. Furthermore, they group small diameter sensory axons together, namely C-fibers, and form Remak bundles, which have a role in nociception (Shir and Seltzer, 1990). MSCs, on the other hand, form a myelin sheath by wrapping around a single large diameter axon. In this process, Schwann cells first form a thin layer around a group of axons and then, they start to proliferate. Axon-Schwann cell contact initiates radial sorting. Consequently, Schwann cells wrap a single axon and form myelinated fibers (Garbay *et al.*, 2000; Scherer and Arroya, 2005).

1.2. Charcot-Marie-Tooth Disease

Charcot-Marie-Tooth (CMT) disease is the most common inherited peripheral neuropathy, with a prevalence of 1 in 2500 (Skre *et al.,* 1974). CMT is also known as hereditary motor and sensory neuropathy (HMSN) since it affects both motor and sensory neurons. The disease is genetically heterogeneous and so far approximately 40 genes and

loci have been associated with CMT. However, over 90% of patients carry mutations in PMP22, GJB1, MPZ or MFN2 genes (Siskin *et al.,* 2013; Vallat *et al.,* 2013). Progressive sensory loss, weakness, muscle atrophy, loss of deep tendon reflexes and foot deformities are examples of observed clinical features of the disease (Harding and Thomas, 1980).

On the basis of nerve conduction studies and histopathology, CMT is classified as demyelinating and axonal neuropathy. Intermediate form of the disease is described recently, describing patients with mixed features. Although motor nerve conduction velocity (MNCV) of median nerve is normally around 45 m/s, patients diagnosed with demyelinating CMT have MNCV lower than 38 m/s (Dyck *et al.*, 1993). Onion bulbs, which are formed due to segmental demyelination and remyelination, are observed in the nerve biopsies of demyelinating CMT cases (Hsieh *et al.*, 2003). Many genes have been associated with this subtype of CMT and their mutations ultimately affect the myelination process. The most common mutation is 1.4-Mb duplication of the region on chromosome 17 containing the peripheral myelin protein (PMP22) gene with a frequency of 67%. This duplication segregates as an autosomal dominant (AD) trait and MNCV is lower than 35 m/s in these patients due to demyelination (Lupski *et al.*, 1991; Nelis *et al.*, 1996).

The second major category of CMT is axonal CMT (CMT2) with AD segregation where MNCV is slightly lower or normal. However, the amplitude of compound muscle action potential (CMAP) is reduced or cannot be measured at all in CMT2 cases. As for demyelinating CMT, the histopathology of CMT2 patients reveals perturbations of the neuronal network and instead of onion bulb formations, axonal loss is observed. Compared to CMT1, CMT2 is genetically more heterogeneous with at least 10 causative genes. Patients with intermediate form of the disease exhibit MNCV between 25-45 m/s and share features of both demyelinating and axonal neuropathy (Zuchner and Vance, 2006).

Since many genes associated with CMT the mechanisms causing the disease are diverse and affect many distinct cellular and molecular processes. Demyelination and axonal degeneration might occur through several mechanisms such as impairment of mitochondrial network dynamics and membrane trafficking. Furthermore, disturbed interaction between Schwann cells and axons might be responsible for the disease phenotype (Bucci *et al.,* 2012; Zuchner and Vance, 2006).

1.3 Ganglioside-Induced Differentiation-Associated Protein 1

Ganglioside-induced differentiation-associated protein 1 (*GDAP1)* is located on chromosome 8q21.11 and is covering an approximately 24 kb region with its six exons. The gene is ubiquitously expressed, but its expression is predominant in the tissues of the nervous system (Cuesta *et al.,* 2002; Niemann *et al.,* 2005; Pedrola *et al.,* 2008). Interestingly, *GDAP1* mutations cause demyelinating, axonal or intermediated subtypes of CMT with recessive and dominant segregation (Casserau *et al.,* 2011). It encodes for GDAP1 protein that belongs to the ganglioside-induced differentiation-associated protein family. The protein is localized to the mitochondrial outer membrane (MOM) (Niemann *et al.,* 2005; Pedrola *et al.,* 2008). It has five domains: two glutathione S-transferase (GST) domains (GST-N and GST-C), a hydrophobic domain (HD), a transmembrane domain (TMD) and an α4-α5 loop (Figure 1.1) (Marco *et al.,* 2004, Niemann *et al.,* 2009). Studies performed in the light of these findings implicated its involvement in oxidative stress mechanism and mitochondrial network dynamics.

Figure 1.1. Domains of GDAP1.

Perturbation in mitochondrial network dynamics and oxidative stress mechanisms are one of the major causes of neurodegenerative diseases. Since *GDAP1* is known to be involved in both of these processes, studying the function of *GDAP1* does not only shed light on these processes, but also may help unraveling the CMT disease mechanism.

1.3.1. Glutathione S-Transferase

GSTs are one of the most abundant and ubiquitously expressed proteins in humans and they have a vital role in oxidative stress mechanism. They function as glutathione peroxidases and regulate various molecular processes. Besides, GSTs are responsible for neutralization of many chemicals harmful for the cell, including reactive oxygen species (ROS) and xenobiotics, by conjugating them to glutathione (Board and Menon, 2013).

When GDAP1 was first identified, it was thought to be an important member of the oxidative stress mechanism since bioinformatics analyses indicated presence of two GST domains. Together with ganglioside-induced differentiation-associated protein 1 like 1 (GDAP1L1), GDAP1 is categorized as a novel subfamily of GST-like proteins although they have close sequence similarity to cytosolic GSTs. This different categorization is based on the fact that both GDAP1 and GDAP1L1 have a TMD and an α4-α5 loop (Marco *et al.,* 2004). In the initial experiments performed by different groups, recombinant forms of GDAP1 did not show any GST activity *in vitro*. The recombinant protein used in the study may not reflect the *in vivo* activity of the wild type GDAP1 since it one had no transmembrane domain (Shield *et al.,* 2006).

The finding that GDAP1 is localized to the mitochondrial outer membrane suggested that it may have a function in mitochondrial dynamics, rather than directly affecting oxidative stress mechanisms. However, recent studies have shown that GDAP1 displays GST activity as its knockdown increases susceptibility to oxidative stress-caused death and its overexpression has oxidative stress lowering effects in neurons. In addition, similar findings in the fibroblasts of a CMT4A patient support the function of GDAP1 as a GST and a regulator of oxidative stress (Noack *et al.,* 2012).

1.3.2. Mitochondrial Network Dynamics

Mitochondria provide the energy required for proper cellular functioning. Contrary to what is believed, they have dynamic structures and undergo fusion and fission processes constantly (Chen and Chan, 2009). These continuous processes preserve mitochondrial function by keeping in balance the morphology, size and number of mitochondria. Furthermore, fusion and fission mechanisms contribute to mitochondrial motility within the cell (Berman *et al.,* 2008).

Mitochondrial network dynamics is regulated by several factors. Mitofusins (Mfn1 and Mfn2) and optic atrophy protein 1 (Opa1) are required for fusion of mitochondria. Mitofusins are anchored to the MOM while OPA1 is located on the inner membrane of mitochondrion. These two types of GTPases are responsible for fusion of inner and outer membranes of mitochondria, respectively. Fusion of both inner and outer membranes

occurs simultaneously in wild type cells. Dynamin-related protein 1 (Drp1) and fission 1 (Fis1) are required for fission of mitochondria. Drp1 is located in the cytosol and it has to be recruited to the mitochondrion in order to initiate the fission process. Fis1, mitochondrial fission factor (Mff), mitochondrial dynamic protein of 49 kDa (MiD49) and mitochondrial dynamic protein of 51 kDa (MiD51) are responsible for recruiting Drp1 to the mitochondrion. It is thought that Drp1 acts as a GTPase and its function is to constrict and break up the mitochondrial membrane into two causing fission (Chen and Chan, 2005).

Mitochondrial network dynamics keep the organelle healthy and functional. Continuous fusion and fission provide content exchange among mitochondria. This dynamic structure keeps the mitochondria homogenous by preventing the aggregation of ROS and mutated mtDNA in a single mitochondrion. Therefore, any imbalance in these processes might lead to several events such as cellular stress and apoptosis.

As neurons consume more energy compared to other cell types, balanced dynamics of mitochondria is crucial for their proper functioning and survival. So far, in several neurodegenerative diseases such as CMT and Huntington's disease, alterations in mitochondrial network dynamics have been observed (Chen & Chan, 2009). Mutations associated with *Mfn2* (mitochondrial fusion) and *GDAP1* (mitochondrial fission) are known to cause CMT (Siskind *et al.,* 2013).

Among the CMT-causing genes, *GDAP1* is an important member; however, there is relatively limited information about it. GDAP1 is a tail-anchored (TA) protein. Two possible models have been suggested to explain the positioning of GDAP1 on MOM; either only TMD or both TMD and HD are anchored to MOM (Figure 1.2). However, the details have still to be resolved. TMD is thought to mediate transportation and anchorage of GDAP1 from cytosol to mitochondria (Wagner *et al.,* 2009).

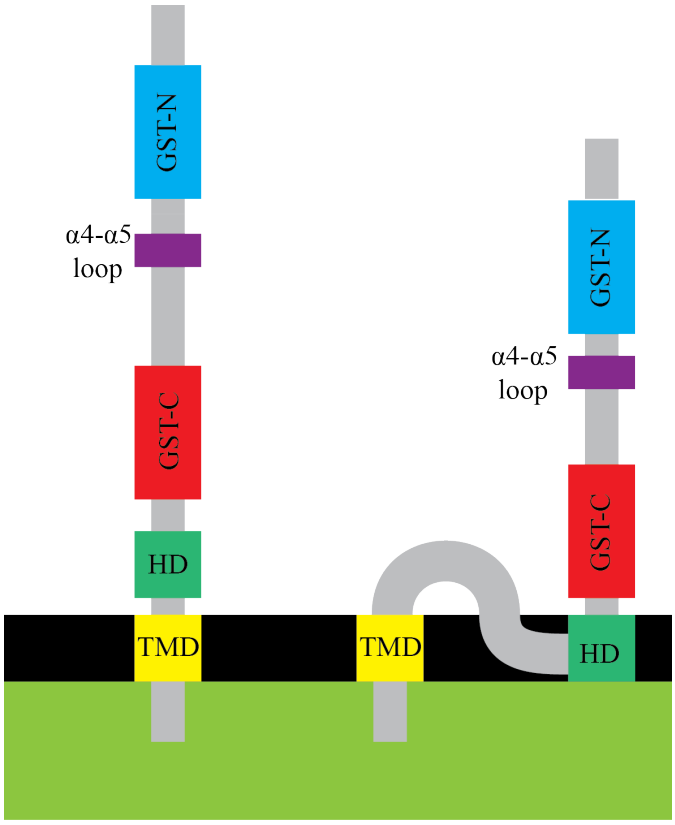

Figure 1.2. Hypothetical GDAP1 positioning on MOM. Represented domains are GST-N (blue), α4-α5 loop (dark magenta), GST-C (red), HD (green) and TMD (yellow).

The overexpression of GDAP1 has been shown to induce mitochondrial fragmentation; however, it does not affect overall mitochondrial activity or interfere with mitochondrial fusion mechanisms. Besides, this fragmentation process does not induce apoptosis. In other experiments, an increase in tubular and elongated mitochondria have been observed, when GDAP1 was down-regulated with RNA interference. These findings suggested GDAP1 as a key regulator of mitochondrial network dynamics (Niemann *et al.,* 2005); however, Fis1 and Drp1 are also required for GDAP1-induced fission function. It is also known that GDAP1 is interacting with the tubulin beta class I (TUBB), a β-tubulin, and also takes part in mitochondrial motility together with RAB6B and caytaxin (Pla-Martin *et al.,* 2013).

1.3.3. GDAP1 is a Causative Gene of CMT

CMT patients with GDAP1 mutations present clinical heterogeneity. GDAP1 mutations cause both demyelinating and axonal CMT as well as the intermediate form.

Furthermore, both autosomal recessive and dominant segregation is possible, although the majority of its mutations segregate recessively. CMT mutations associated with GDAP1 cause generally severe phenotypes with early onset except for dominant mutations. Clinical findings of these patients are diverse including all hallmarks of CMT: progressive sensory loss, weakness, muscle atrophy, loss of deep tendon reflexes and skeletal deformities. Onset of the disease is in the first few years and the patients lose their ambulatory capacity by the second decade. Additional features are vocal cord and diaphragm paralysis, facial weakness and hoarseness of the voice (Wagner *et al.,* 2009; Cassereau *et al.,* 2011).

Most GDAP1 mutations are recessive and therefore can be thought of as loss of function mutations. The fact that they cause a severe phenotype shows its requirement for proper development and maintenance of the motor and sensory system. As their effect is less severe, dominant mutations of GDAP1 are thought to be gain of function mutations, which do not perturb the cellular dynamics as much as recessive ones.

1.3.4. *CG4623* is the *Drosophila melanogaster* Homolog of *GDAP1*

Among vertebrates GDAP1 is highly conserved and GDAP1 homologs are present in invertebrate species (Marco *et al.*, 2004). Even though the overall homology for this gene decreases with phylogenetic distance, the gene is still conserved with its major domains. Bioinformatics analyses showed that *CG4623* is the *Drosophila* homolog of GDAP1 and GDAP1L1 genes. GDAP1 and CG4623 share 49% similarity and 31% identity at the amino acid level (Altschul *et al.,* 1997; Altschul *et al.,* 2005). However, the function of CG4632 is not known, yet.

The *CG4623* gene is located on the left arm of the third chromosome. Its length is 2.4 kb and it has four exons and two alternatively spliced transcripts. Both GDAP1 and GDAP1L1 have two conserved GST domains (Figure 1.3). Since *CG4623* has not yet been studied thoroughly, its expression profile is not clearly known.

Figure 1.3. Conserved domain structures of GDAP1 and CG4623.

1.4. *Drosophila melanogaster* as a model organism

The fruit fly *Drosophila melanogaster* has been used for years to unravel many biological processes as well as to understand the mechanisms underlying many diseases. The works of Thomas Hunt Morgan during the first decades of 18th century made *Drosophila* as one of the major model organisms in the scientific research. He devised a methodology to assess the distance between genes and their location on chromosomes using Drosophila as the model. Since 1900s, *Drosophila* genetics has developed extensively. Its genome has been fully sequenced (Adams *et al.,* 2001) and it is well annotated. Furthermore, there are various genetic tools generated for studying molecular processes, such as yeast GAL4-UAS binary system or P-elements and other transposons.

Among the reasons for popularity of *Drosophila* as a model organism, is its anatomy and ease of handling. The life cycle of *Drosophila* is very short at 25°C. After fertilization, the larvae hatch from their eggs and three to four days later they start to climb the walls of the vials during the third instar stage. With the pupariation that starts at the fifth day, they undergo metamorphosis. From fertilization to fertile adulthood, it takes approximately 10 days.

Many important biological mechanisms are well conserved between *Drosophila* and mammalian species. Approximately 75% of genes mutated in human diseases have at least one *Drosophila* homolog (Pandey and Nichols, 2011). Hence, it is used to generate disease models for many disorders such as ALS and Parkinson's disease to shed light on mechanisms responsible for disease phenotype and finding therapeutic agents to be tested on mammalian models.

1.4.1. The Nervous System of *Drosophila melanogaster*

The nervous system of *Drosophila* at the larval stage consists of a central nervous system with two brain lobes and ventral nerve cord (VNC) along with an extensive peripheral nervous system (Figure 1.4). Motor neurons stem from the VNC and migrate to the muscles to form neuromuscular junctions (NMJ). Similarly, sensory neurons convey the information from the peripheral nervous system to the VNC.

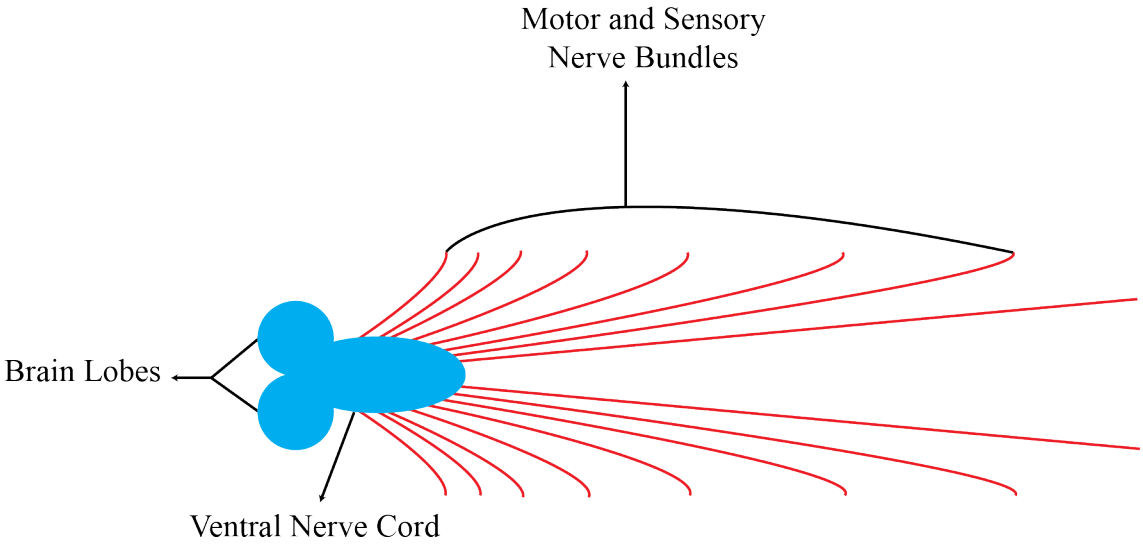

Figure 1.4. Larval nervous system of *Drosophila melanogaster*.

Although *Drosophila melanogaster* has no myelin structure like the one observed in mammalians, it has a similar ensheathing structure surrounding peripheral neurons. Their function may not be the same as for mammalian myelin. Motor and sensory neurons are enclosed by three layers of peripheral glial cells (Figure 1.5). First, axons are ensheathed by wrapping glia and this forms a structure similar to the Remak bundle in mammals. On top of this layer, subperineurial glia wraps this structure and then perineurial glia form the outermost layer. Therefore, despite apparent differences, this overall structure can be used as a model for studying peripheral neuropathy.

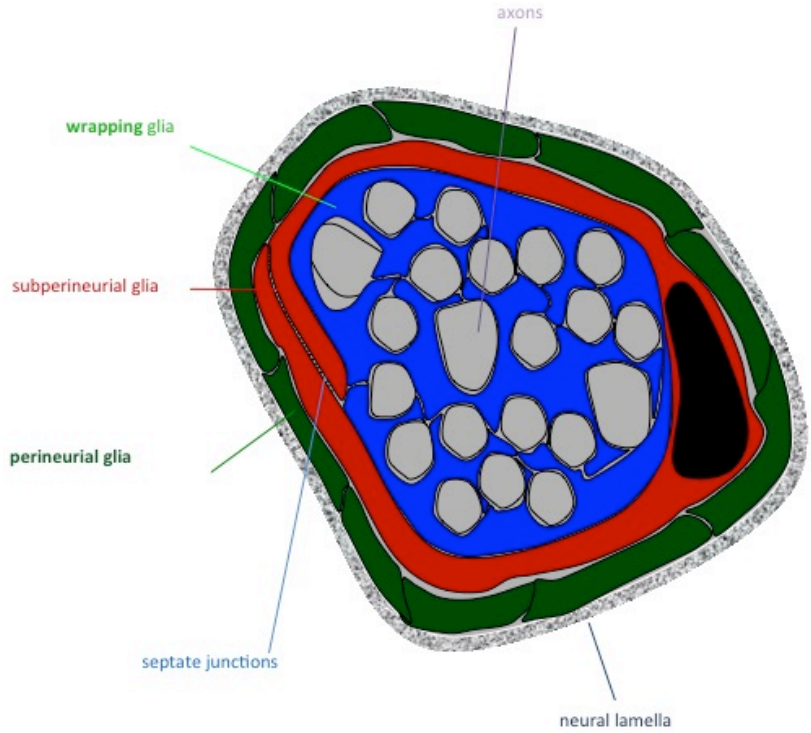

Figure 1.5. Larval sensory and motor neurons enclosed by three layers of glia. Represented structures are axons (grey), wrapping glia (blue), subperineurial glia (red) and perineurial glia (green).

1.4.2. The Eye of *Drosophila melanogaster*

The eye of *Drosophila melanogaster* consists of approximately 800 symmetrically organized units, which are known as ommatidia (Ready, 1978). An ommatidium is formed of eight photoreceptor cells (PR), which send their axons to the brain and 12 accessory cells. Glial cells derived from the brain guide this axonal migration. The adult organs of *Drosophila melanogaster* develop from several imaginal discs, which are epithelial sheets of differentiated and undifferentiated cells (Figure 1.6). Eye-antennal imaginal disc is one of them and adult eye and antenna are developed from this structure.

Differentiation in the eye imaginal disc starts with the initiation of morphogenetic furrow at the posterior part of the eye disc. It sweeps through the disc to the anterior part by leaving differentiated cells posterior to it. This differentiation occurs sequentially, so the cells at the posterior are the ones that complete their differentiation first. Therefore, the eye imaginal disc is an excellent model for studying neurodegenerative disorders as it has a

very precise pattern that may be affected by neurodegeneration and there are different types of cells that may be prone to degeneration to various extents (Curtiss and Mlodzik, 2000).

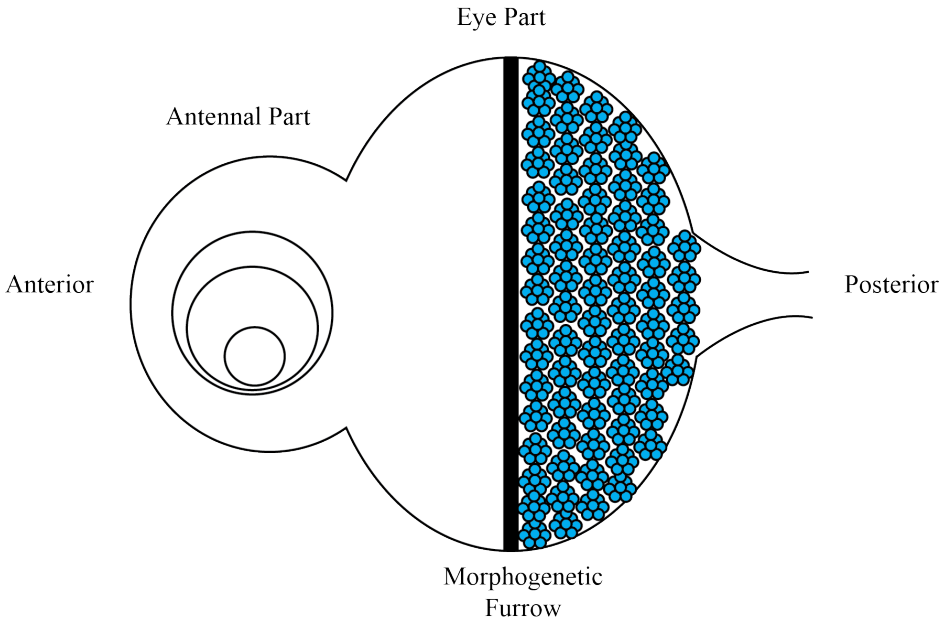

Figure 1.6. Eye-antennal imaginal disc.

1.4.3. The GAL4/UAS Binary System

The GAL4/UAS system is a well-established technique for spatial and temporal expression of a gene of interest (Brand and Perrimon, 1993). This binary system was first identified in *Saccharomyces cerevisiae* and it consists of two components, GAL4 and UAS. GAL4 is a regulatory protein and is inducible by galactose. It activates the transcription by binding a specific upstream activator sequence (UAS). Besides these two components, GAL80 can also be used in this system. GAL80 is usually expressed under a temperature sensitive promoter and binds to GAL4 inhibiting its transcriptional activation function (Duffy, 2002).

The Gal4/UAS system has been used in *Drosophila* for about 20 years in genetic analyses (Brand and Perrimon, 1993). For these analyses, GAL4 is cloned into downstream region of the promoter/enhancer of a gene, replacing the gene and allowing expression of the GAL4 specifically in a certain tissue or developmental time point. On the other hand,

the target gene is cloned downstream of a UAS element. Therefore, GAL4 expression is necessary for the expression of the gene of interest under UAS control and this can be achieved by bringing them together in the same background.

This technique can also be used for the down-regulation of a gene in a time and tissue specific manner. Inverted repeats of 300 – 400 bp specific to an mRNA of interest are cloned downstream of an UAS. Upon activation with GAL4, this short hairpin RNA (shRNA) is transcribed and processed into double stranded siRNAs. The siRNA generated provides the degradation of the target mRNA, causing down-regulation of the gene. However, in some cases transcription of siRNA is not efficient for proper down-regulation. In that case, UAS-Dicer-2 responder element is also included in the genome to enhance RNAi potency (Dietzl *et al.,* 2007) (Figure 1.7). Today, there are many GAL4 and UAS lines including RNAi libraries that are commercially available through several stock centers.

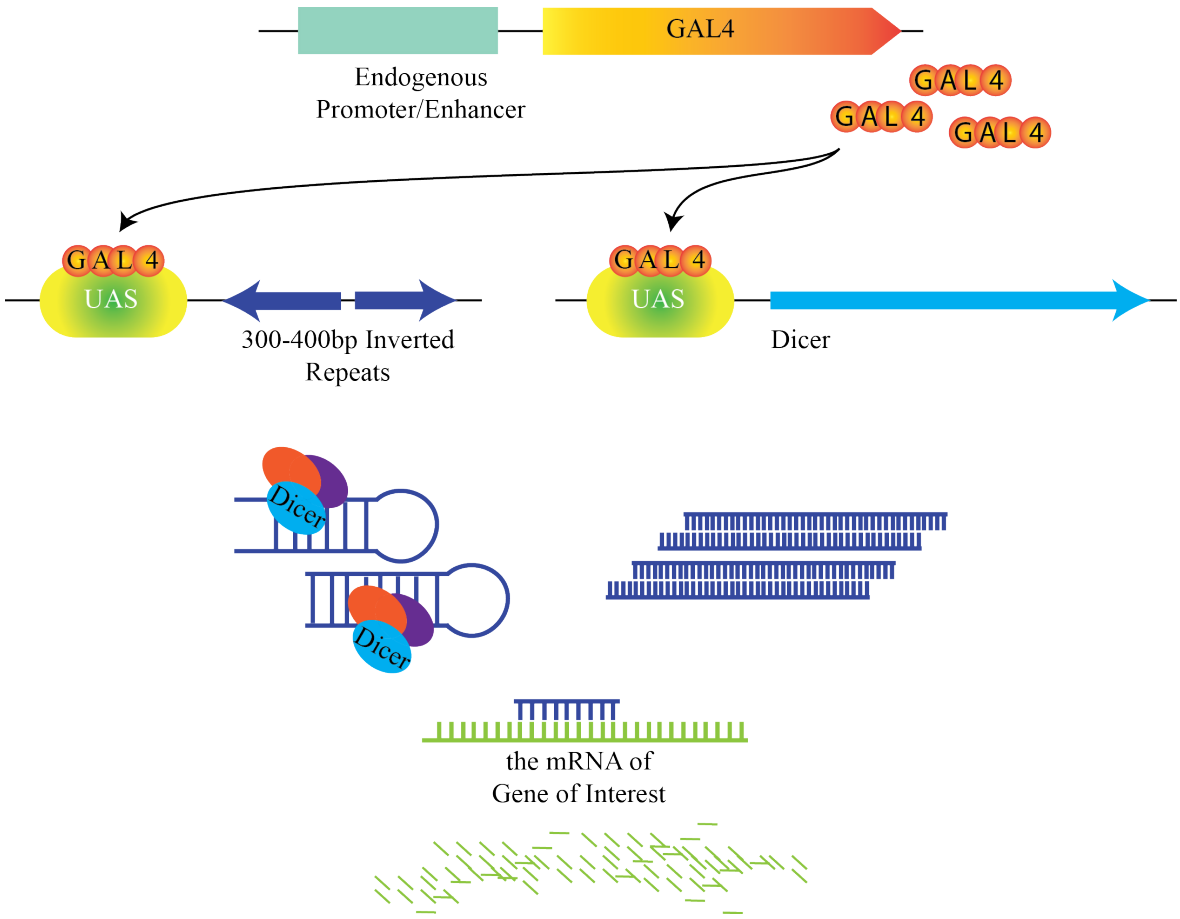

Figure 1.7. Down-regulation of a gene of interest using the GAL4/UAS binary system.

1.5. Integrase-mediated Approach for Gene Knockout (IMAGO)

Homologous recombination is a mechanism that has been widely utilized to knockout and knock-in genes of interest in various model organisms. The ends-out homologous recombination system is a powerful tool in *Drosophila melanogaster* as this system allows a construct to be integrated randomly into the genome and be linearized using heat shock-activated I-*SceI* and flippase enzymes (Figure 1.8) (Rong and Golic, 2003). The linearized DNA fragments generated in this way align to regions with high homology and a potential homologous recombination event will occur and allow for exchange of this construct with the targeted endogenous sequence. A major drawback of the homologous recombination is that this event is rare. In addition, it is difficult to clone large regions of homology arms, although they increase the efficiency of recombination.

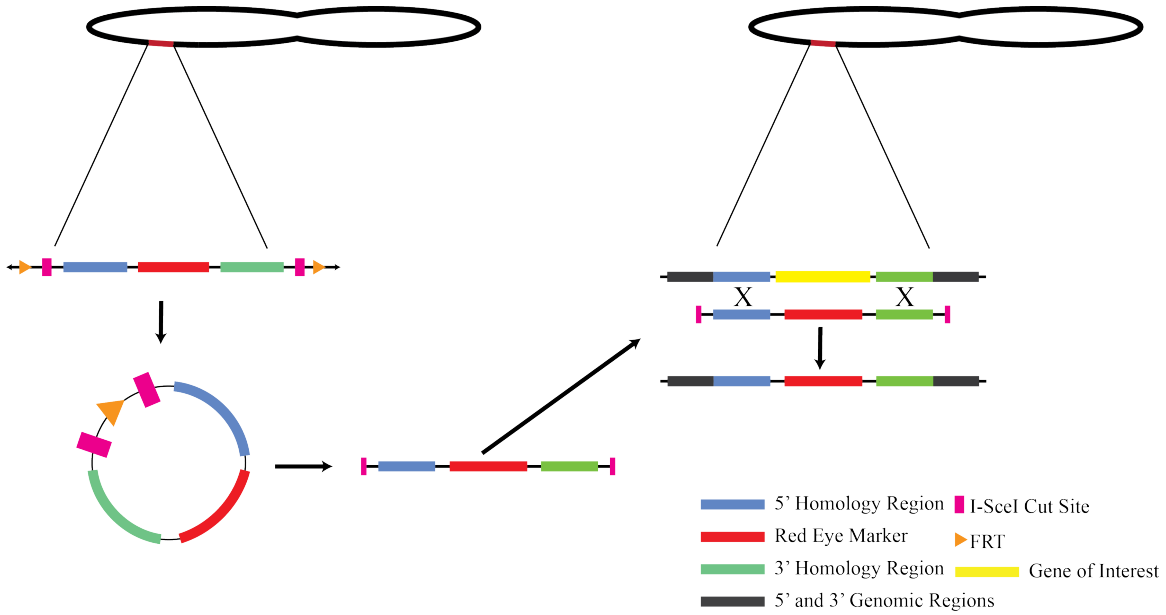

Figure 1.8. Ends-out homologous recombination.

The integrase-mediated approach for gene knockout (IMAGO) is a further development of the ends-out homologous recombination technique. This system allows the site-specific integration of the construct. It is also possible to knock-in any gene of interest by using integrase mediated cassette exchange (RMCE) (Figure 1.9). This is possible because the targeting construct includes phage attachment sites (attP) flanking the gene to be knocked-in, which is initially the red eye marker. Using attP sites, any coding sequence

of interest flanked by attB sites could be used to replace the sequence between the two attP sites and this is efficiently done by RMCE (Choi *et al*., 2009).

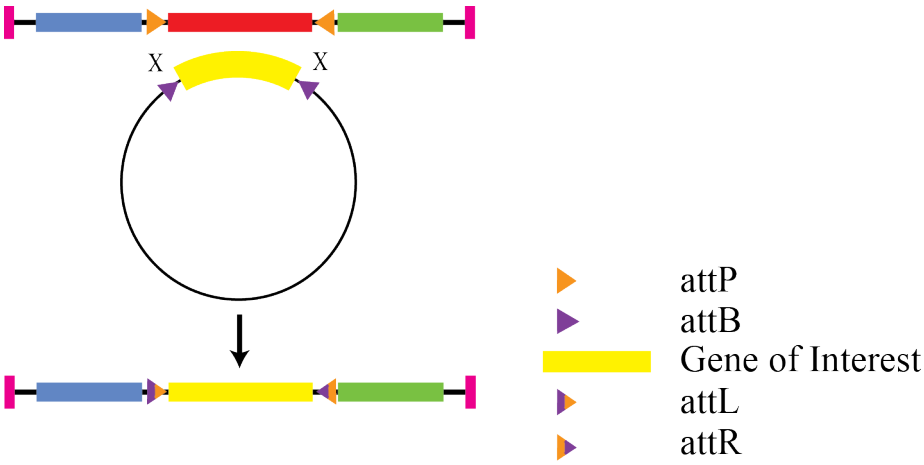

Figure 1.9. Use of attP sites for the IMAGO system.

The IMAGO system simplifies recombination events once a knockout line is obtained because after this point, it does not rely on the flies' internal dynamics of homologous recombination. In order to replace the marker gene, that has previously replaced the target gene, RMCE can be used. Using this system site-specific recombination can be induced efficiently between attB and attP sites, allowing the exchange of any sequence of varying lengths (Choi *et al.,* 2009).

2. AIM OF THE STUDY

Charcot-Marie-Tooth (CMT) disease is the most common peripheral neuropathy with a prevalence of 1 in 2500. It is a genetically and clinically heterogeneous disease with at least 40 genes and loci identified up to date. *GDAP1* mutations cause different subtypes of CMT with recessive or dominant segregation and there is evidence for its involvement in mitochondrial network dynamics and oxidative stress. Moreover, *GDAP1* mutations are the most frequent cause of demyelinating recessive subtype of CMT (CMT4A). However, how *GDAP1* mutations lead to the disease phenotype remains unclear.

Our aim in this study is to develop a *Drosophila* CMT model by silencing the fly homolog of *GDAP1*, *CG4623*, using two different molecular approaches.

In the first part, we have down-regulated *CG4623* ubiquitously and in a tissue specific manner using RNA interference method. Since GDAP1 gene mutations were shown to affect mitochondrial morphology previously in *in vitro* studies RNAi lines generated were subsequently analyzed for changes in mitochondrial morphology. Use of imaginal eye discs and ventral nerve cord as models to study their morphology was investigated.

In the second part of the project, we aimed to generate *CG4623* knockout flies using integrase-mediated approach for gene knockout (IMAGO). The technique allows precise excision and replacement of the target gene with a marker gene that can be replaced by other target genes consequently. Thus, we aimed to generate the target construct and transfer it to a *Drosophila* chromosome *via* microinjection to embryos. Through this approach, in future studies we will be able to introduce *GDAP1* mutations into IMAGO flies and investigate the disease pathophysiology.

3. MATERIALS AND METHODS

3.1. Biological Materials

Drosophila melanogaster flies were raised in the commercially available fly medium (Nutri-Fly^{TM} Bloomington Formulation) supplemented with 4.8 ml of propionic acid per liter. All the fly stocks were kept in the incubators, which were set to 25°C with 80% humidity and 12:12 day:night cycle, unless stated otherwise. Virgin flies were collected 0-4 hour after eclosion and crossed to male flies. Flies used in this study, and their relevant genotype and phenotype, are listed in the Table 3.1. The marker phenotypes of the *Drosophila melanogaster* used in this study are represented in Figure 3.1, 3.2, 3.3, 3.4, 3.5 and 3.6. These images are the courtesy of Dr. H. Bahar Şahin.

Table 3.1. *Drosophila melanogaster* lines used in this study.

Name of Line	Chromosome	Description
General Stocks		
w^{1118}	I	White eye
y, w	I	Yellow body color and white eye
FM7a	I	Balancer chromosome
Sp	II	Supernumerary bristles
CyO	II	Balancer chromosome with Curly wing
CyO, Roi	II	Balancer chromosome with Curly wing and rough eye
CyO, GFP	II	Balancer chromosome with rough ubiquitous GFP expression
Sco	II	Missing bristles scutellum
TM2	III	Balancer chromosome (Bigger haltere, bristle)
TM3, sb	III	Balancer chromosome, shorter bristles
TM3, hs:hid	III	Balancer chromosome, heat shock lethal
TM6B, hu, tb	III	Balancer chromosome, additional macrochaetas on the humeri, shorter and thicker body
IMAGOCGL1	I	pP{White-STAR} vector is integrated on the 1st chromosome

Table 3.1. *Drosophila melanogaster* lines used in this study (cont.).

IMAGOCGL2	I	pP{White-STAR} vector is integrated on the 1st chromosome
UAS Constructs		
UAS-Dcr-2	I	Expresses Dicer-2 under UAS control
UAS-CG4623RNAi	II	Expresses double stranded siRNAi of *CG4623* under UAS control
UAS-mitoGFP	II	Expresses GFP with mitochondrial import signal
UAS-CG4623RNAi, UAS-mitoGFP	II	Expresses double stranded siRNAi of *CG4623* and GFP with mitochondrial import signal under UAS control
GAL4 Lines		
elav-GAL4	II	Expresses GAL4 in the nervous system
Act5C-GAL4	II	Expresses GAL4 ubiquitously
Repo-GAL4	III	Expresses GAL4 in glia

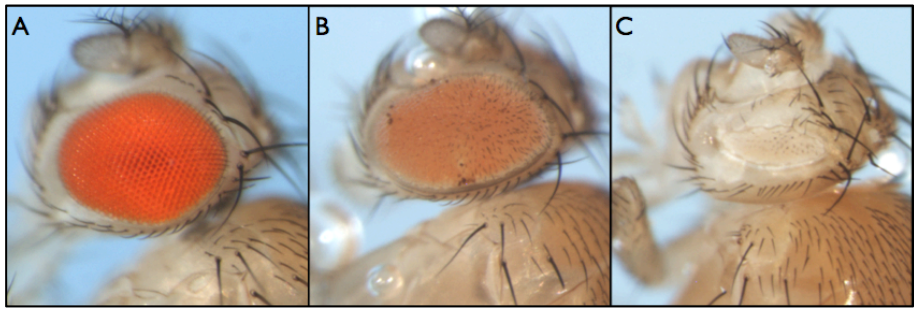

Figure 3.1. The eye markers of *Drosophila melanogaster* used in this study. Images are from wild type (A), rough eye (*Roi*) (B) and *FM7a* (C) flies.

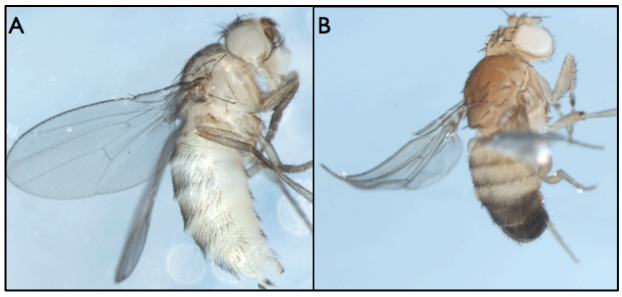

Figure 3.2. The wing marker of *Drosophila melanogaster* used in this study. Images are from wild type (A) and curly wing (*CyO*) (B) flies.

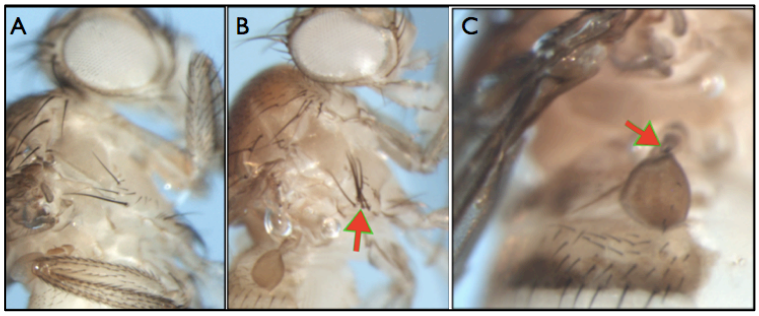

Figure 3.3. The bristle and haltere markers of *Drosophila melanogaster* used in this study. Images are from wild type (A), supernumerary bristles (*sp*) (B) and bigger haltere with bristle (*TM2*) (C) flies.

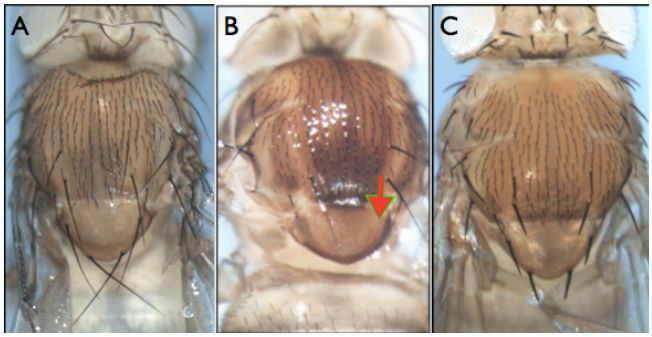

Figure 3.4. The thoracic markers of *Drosophila melanogaster* used in this study. Images are from wild type (A), missing bristles scutellum (*Sco*) (B) and shorter bristles (*TM3, sb*) (C) flies.

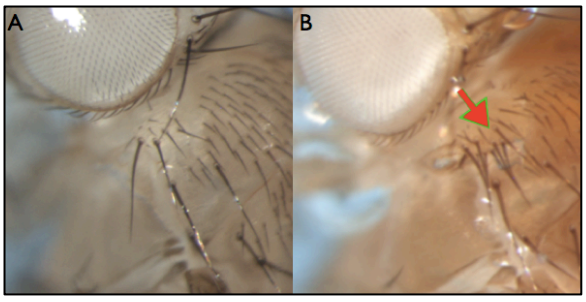

Figure 3.5. The macrochaetas marker of *Drosophila melanogaster* used in this study. Images are from wild type (A) and additional macrochaetas on the humeri (*hu*) (B) flies.

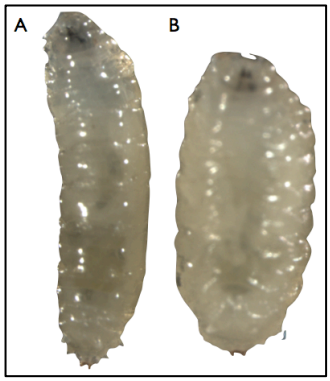

Figure 3.6. The tubby marker of *Drosophila melanogaster* used in this study. Images are from wild type (A) and shorter and thicker larvae (*tb*) (B).

3.2. Chemicals

Chemicals used in this study were purchased from Sigma (USA), Thermo Scientific (USA) and Life Technologies (USA) unless stated otherwise.

3.2.1. Enzymes

Restriction enzymes and buffers used in the study were from New England Biolabs (NEB) or Thermo Scientific. Phusion High-Fidelity DNA Polymerase was purchased from New England Biolabs. *Taq* DNA Polymerase was purchased from Thermo Scientific.

3.2.2. Chemical Supplies

The chemical supplies used in this study are stated in the Table 3.2.

Table 3.2. Suppliers of the chemicals used in this study.

Chemical	Supplier
β-mercaptoethanol	Sigma-Aldrich, USA (T7024)
1 kb DNA Ladder	Thermo Scientific, USA (#SM0311)
1 kb Plus DNA Ladder	Life Technologies, USA (10787-018)
Agarose	Prona Agarose, Biomax, EU (124543PR)
Ampicillin	Mustafa Nevzat, Turkey (Ampisina)
Boric acid	Sigma-Aldrich, USA (B8768)

Table 3.2. Suppliers of the chemicals used in this study (cont.).

Bovine Serum Albumin	Sigma-Aldrich, USA (A2153)
$CaCl_2$	Sigma-Aldrich, USA (C3306)
Chloramphenicol	Applichem, Germany (7495)
EDTA	Sigma-Aldrich, USA (34549)
Ethidium Bromide Solution	Sigma Life Sciences, USA (E1510)
Formaldehyde	Sigma-Aldrich, USA (47608)
Glycerol	Sigma-Aldrich, USA (G5516)
Guanidinium Thiocyanate	Sigma-Aldrich, USA (G9277)
Kanamycin	Life Technologies, USA (11815-024)
KCl	Merck, Germany (TA741635)
LB-Agar	Difco, France (244520)
LB-Broth	Difco, France, (244620)
Manganese Chloride	Simga Aldrich, USA (M3634)
$MgCl_2 \bullet 6H_2O$	Carlo Erba Reagenti, Italy (7791186)
$MgSO_4$	Carlo Erba Reagenti, Italy (349859)
MOPS	Sigma Aldrich, USA (M9381)
NaCl	Sigma-Aldrich, USA (S7653)
Normal Goat Serum (NGS)	Millipore, Germany (S26-100ML)
Phenol	Sigma-Aldrich, USA (P4682)
Potassium Acetate	Sigma-Aldrich, USA (P1190)
PBS	Life Technologies, USA (70011-044)
Rubidium Chloride	Sigma Aldrich, USA (R2252)
Silicone Elastomere Kit	Fisher Scientific, UK (NC9644388)
Sodium Acetate	Merck, Germany (1.06265)
Sodium Deoxycholate	Sigma-Aldrich, USA (30970)
Sybr Premix Ex Taq	Takara, Japan (RR420A)
Tris	Sigma-Aldrich, USA, (T1503)
Triton X-100	Sigma-Aldrich, USA (T8787)
Tryptone	Conda, Spain (1612.00)
Yeast extract	Merck, Germany (1.037.53)
VectaShield Mounting Medium	Vector Laboratories, USA (H-1000)

3.2.3. Buffers and Solutions

The buffers and solutions used in this study are stated in the Table 3.3 and Table 3.4.

Table 3.3. Contents of buffers and solutions used in molecular biology experiments.

Buffer/ Solution	Content
1% Agarose Gel	1X TAE Buffer 1% Agarose 0.5% Ethidium Bromide
Elution Buffer	10 mM Tris-Cl, pH 8.5
Ethidium Bromide Solution	10 mg/ml
LB Broth	5 g/l NaCl 10 g/l Tryptone 5 g/l Yeast Extract
LB Agar	5 g/l NaCl 10 g/l Tryptone 5 g/l Yeast Extract 15 g/l Agar
P1 (Resuspension Buffer)	50 mM Tris-Cl, p H 8.0 10 mM EDTA 100 µg/ml RNase A
P2 (Lysis Buffer)	200 mM NaOH 1% SDS (w/v)
P3 (Neutralization Buffer)	3.0 M Potassium Acetate, pH 5.5
Super Optimal Broth with Glucoase (SOC)	2g Tryptone 0.5 g Yeast Extract 0.05 g NaCl 1 M KCl 1 M $MgCl_2$ 1 M $MgSO_4$ ddH_2O to 100 ml
1X TAE Buffer	40 mM Tris-HCl 1 mM EDTA 0.1% Acetic Acid
Transformation Buffer 1 (TFB1)	100 mM RbCl 50 mM $MnCl_2$•H_2O 30 mM Potassium Acetate 10 mM $CaCl_2$•H_2O 15% Glycerol
Transformation Buffer 2 (TFB1)	10 mM RbCl 10 mM MOPS 75 mM $CaCl_2$•H_2O 15% Glycerol

Table 3.3. Contents of buffers and solutions used in molecular biology experiments (cont.).

2X YT Media	16 g Bacto Tryptone 10 g Bacto Yeast Extract 5 g NaCl

Table 3.4. Contents of buffers and solutions used in immunohistochemistry assays.

Buffer/ Solution	**Content**
PAXDG (for 1 liter)	10 g BSA 3 g Sodium Deoxycholate 3 ml Triton X-100 50 ml NGS 100 ml 10X PBS 850 ml dH_2O
1XPBS (for 1 liter)	100 ml 10X PBS 900 ml ddH_2O
PBX3 (for 1 liter)	1X PBS 0.3% Triton X-100

3.2.4. Oligonucleotide Primers

Lyophilized primers were resuspended in sterile water with a final concentration of 100 mM and then stored at -20 °C. Restriction sites in the primers were shown in red and lowercase letters. Oligonucleotide primers used in this study are stated in Table 3.5.

Table 3.5. Sequences and annealing temperatures of primers used in this study.

Primer Name	**Primer Sequence (5' - 3')**	**T_m°C**
CG4623_5HF	ggtaccGGTGAAGGAGCGCCCGTATGAC	69°C
CG4623_5HR	cctaggTTTCGCGCCACCGGCGAATGAG	70°C
CG4623_3HF	gctagcGCTCTCCCCTCTGTTGAC	64°C
CG4623_3HR	ccgcggCGGGCACTCCATCAGATC	69°C
CG4623_5HS1	CTTGGCTTCATCCTCCGTCT	58°C
CG4623_5HS2	ACTCCTATAGCGCCAATCGA	57°C
CG4623_5HS3	CAACAAGGTGCTCGACGAGA	58°C
CG4623_5HS4	AACCTCAAAGGCATCATAGC	54°C
CG4623_3HS1	AGGCTGCGCATTTGCTCCTC	62°C
CG4623_3HS2	TACTTTGAGGTCCGTATTGA	52°C
CG4623_3HS3	TTTCGTGGCGAATGGCAAGC	60°C

Table 3.5. Sequences and annealing temperatures of primers used in this study (cont.).

CG4623_3HS4	ACAACATTGATCCAGGTCGT	55°C
CG4623_5HRS1	TGTGGACTCTGCTCTGGCGG	63°C
CG4623_5HRS2	AGCAAAATACCCATGGGTCG	56°C
CG4623_5HRS3	TTAGGGCGATATTGGCGCCC	61°C
CG4623_5HRS4	TCGATAATTATTTTCTAAAC	42°C
CG4623_3HRS1	GCACAGCCGTTAGCCGCTCA	64°C
CG4623_3HRS2	CCCAAAGGTCTCGTGAGAAA	56°C
CG4623_3HRS3	AACCCGCTCTTTATAAAAAT	49°C
CG4623_3HRS4	TCATCCATTTGTGCAAGAAG	52°C
IMAGO_CG4623_SCR_F	TGTCCCACACCTTCTCATCGCACTC	64°C
IMAGO_CG4623_SCR_R	AGCGAGCACAGCTACCAGAATAATC	60°C
CG4623_RT1_FP	GCCAATAAGCCAGTGCTCTTC	56°C
CG4623_RT1_RP	GCCCTTGGGATTGAGGTTTAG	56°C
GAPDH2_FP	TGGTACGACAACGAGTTTGG	55°C
GAPDH2_RP	TTTCAGGCCGTTTCTGAAGT	55°C
Actin79b_RT_FP	ATGTATCCAGGTATCGCTGAC	54°C
Actin79b_RT_RP	TGCTTGGAGATCCACATCTG	55°C

3.2.5. Antibodies

Primary and secondary antibodies used in this study, their host species, and the dilutions used are stated in Table 3.6.

Table 3.6. Primary and secondary antibodies used in this study.

Name	Antigen	Species	Dilution	Supplier
Primary Antibodies				
Anti-elav	Elav	Rat	1:50	DSHB
Anti-repo	Repo	Mouse	1:20	DSHB
Anti-GFP	GFP	Rabbit	1:500	Torrey Pines Biolabs
Secondary Antibodies				
Alexa 488	Rabbit	Goat	1:1000	Invitrogen
Alexa 555	Mouse	Goat	1:1000	Invitrogen
Alexa 633	Rat	Goat	1:1000	Invitrogen

3.3. Disposable Labware

Disposable labwares used in this study are stated in the Table 3.7.

Table 3.7. Disposable labwares used in this study.

Disposable Labware	**Supplier**
Centrifuge Tubes, 15 ml	Becton, Dickinson and Company, USA
Centrifuge Tubes, 50 ml	Becton, Dickinson and Company, USA
Culture Tubes, 14 ml	Greiner Bio-One, Belgium
Filter Tips	Fisher Scientific, UK
Microcentrifuge Tubes, 0.5 ml	Fisher Scientific, UK
Microcentrifuge Tubes, 1.5 ml	Fisher Scientific, UK
Microcentrifuge Tubes, 2 ml	Fisher Scientific, UK
Microscope Cover Glass	Isolab, Germany
Microscope Slides	Isolab, Germany
Microseal PCR Sealers	Bio-Rad, USA
Pasteur Pipettes	Isolab, Germany
PCR Tubes (200 µl)	Fisher Scientific, UK
PCR Strips (8 well)	Fisher Scientific, UK
PCR Plates (96 well)	Fisher Scientific, UK
Petri Dishes (60 mm)	Isolab, Germany
Petri Dishes (90 mm)	Isolab, Germany
Pipette Tips	Fisher Scientific, UK
Positively Charged Slides	Thermo Scientific, USA

3.4. Equipment

Equipments used in this study are stated in the Table 3.8.

Table 3.8. Equipments used in this study.

Equipment	**Supplier**
Autoclave	Astell Scientific Ltd., UK
Centrifuges	Centrifuge 5415 (Eppendorf, Germany)
Cold Room	Birikim Elektrik Soğutma, Turkey
Confocal Microscope	TCS SP5 (Leica Microsystems, USA)

Table 3.8. Equipments used in this study (cont.).

Dissection Forceps	FST, USA
Dissection Microscope	SZ61 (Olympus, Japan)
Dissection Scissors	WPI, USA
Electrophoresis Equipment	Mini-Sub Cell (Bio-Rad, USA) PROTEAN Vertical Electrophoresis System (Bio-Rad, USA)
Fluorescence Stereomicroscope	MZ16FA (Leica Microsystems, USA)
Freezers	-20 ºC (Bosch, Germany) -20 ºC (Arçelik, Turkey) -70 ºC (Thermo Forma, USA)
Gel Documentation System	Bio-Rad Labs, USA (Gel Doc XR)
Heating Block	DRI-Block DB-2A (Techne, UK)
Heating Magnetic stirrer	Speed Safe (Hanna Instruments, USA) MK 418 (Nüve, Turkey)
Homogenizer	MagNA Lyser (Roche, Germany)
Fly Incubators	TK 120 (Nüve, Turkey) TK 600 (Nüve, Turkey)
Laboratory Bottles	Isolab, Germany
Light Cycler	LightCycler Carousel Based System (Roche, Germany)
Micropipettes	Gilson, USA
Microwave Oven	Arçelik, Turkey
Spectrometer	NanoDrop ND-1000 (NanoDrop, USA)
Refrigerators	+4º C Arçelik, Turkey
Shaker	SL 350 (Nüve, Turkey)
Stereo Microscope	Olympus, USA (SZ61)
Thermal Cycler	Bio-Rad Labs, USA (C1000 Thermal Cycler)
Vortex Mixer	Nuvemix (Nüve, Turkey)
Water Bath	BM 302 (Nüve, Turkey)

3.5. Experiments for Down-Regulation of *CG4623* in Drosophila

UAS-CG4623RNAi flies were obtained from the Vienna *Drosophila* Resource Center (VDRC) and were crossed with *Act5C-GAL4*, *elav-GAL4* and *Repo-GAL4* for ubiquitous, pan-neuronal, and pan-glial down-regulation of *CG4623*.

3.5.1. Determination of Down-regulation Levels in the Ubiquitously Down-regulated RNAi Lines

To confirm the down-regulation of the gene quantitative reverse transcription PCR was performed. For this purpose, *UAS-CG4623RNAi* flies were crossed with *Act5C-GAL4* flies in order to ubiquitously down-regulate *CG4623* (Figure 3.7). The progeny flies from the cross between wild type flies (w^{1118}) and *Act5C-GAL4* flies were used as control in this experiment.

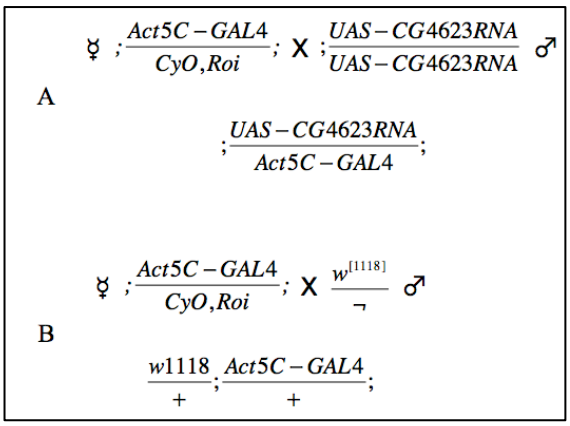

Figure 3.7. Crossing scheme to determine if the RNAi line can down-regulate the levels of *CG4623* (A). As a control, the progenies of the cross between wild type flies (w^{1118}) and *Act5C-GAL5* (B) were used.

3.5.1.1. RNA Isolation. Total RNA was isolated from the heads of 30 five-week-old flies of equal number of males and females using RNeasy Mini Kit (Qiagen, Germany). Briefly, the heads were homogenized in 1 ml 4 M guanidinium thiocyanate (GTC), 1 ml phenol and 7.2 µl β-mercaptoethanol using MagNA Lyser (Rocher, Germany). Chloroform at a Volume of 1:5 was added to the tubes and kept at room temperature for 3 min. After centrifugation at 12000 g for 15 min at 4°C, the upper phase was collected and equal volume of 70% ethanol was added. The sample was transferred to a column placed in 2 ml collection tube and centrifuged for 15 seconds at 8000 g at room temperature. Finally, after extensive washes with provided buffers, RNA was eluted in 40 µl RNase free water. The concentrations of RNA samples were determined using a Nanodrop spectrophotometer.

3.5.1.2. cDNA Synthesis. cDNA was synthesized using RevertAid first strand cDNA synthesis kit (Thermo Scientific, USA). Each reaction was performed in a total volume of 20 µl, including template RNA (11 µl from previous step), 1 µl oligo $(dT)_{18}$ primer, 4 µl 5X reaction buffer, 1 µl RNase inhibitor, 2 µl 10 mM dNTP mix and 1 µl of reverse transcriptase. The mixture was incubated for 60 min at 42°C and the reaction was terminated by heating at 70°C for 5 min.

3.5.1.3. Quantitative Real Time PCR. Quantitative real time PCR reactions were performed in a volume of 20 µl containing 2 µl of cDNA sample, 10 µl of 2x SYBR Premix Ex Taq (Takara, Japan), 0.4 µl of CG4623_RT1 or actin79b_RT primer pairs (stock concentration: 5 µM each) and 7.2 µl of dH2O. Reaction mixtures were prepared for both target and reference genes. Actin79b was used as the reference gene because expression of this gene was shown to be highly stable in different tissues. The qRT-PCR program on Light Cycler (Roche Diagnostics, Manheim, Germany) was as follows: an initiation step at 50°C for 2 minutes, followed by an initial denaturation step at 95°C for 10 seconds, followed by 40 cycles (with possible extension of 10 more cycles) of 5 seconds at 95°C, 10 seconds at 55°C, 10 seconds at 72°C (with single acquisition of signal using channel 530 at this step), a melting curve construction step and a cooling step at 40°C for 30 seconds. Data was analyzed via the LightCycler Software 4 and qRT-PCR results of RNAi cDNA samples were evaluated with comparative threshold cycle (CT) method. For comparison, the experiments were performed in triplicates for three cDNA samples for control and RNAi flies with both CG4623_RT and actin79b_RT primers for each sample.

3.5.2. The Recombination of *UAS-CG4623RNAi* and *UAS-mitoGFP*

The RNAi line for *CG4623* and GFP reporter line for mitochondria were UAS lines expressed from chromosome 2. Thus, we decided to produce flies that have both genes in *cis* on the same chromosome in order to analyze mitochondrial morphology upon down-regulation of *CG4623*. The crossing scheme used for this purpose is represented in Figure 3.8.

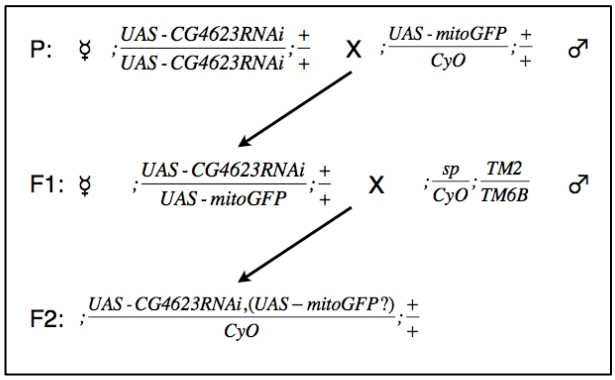

Figure 3.8. Crossing scheme for the recombination of *UAS-CG4623RNAi* and *UAS-mitoGFP* lines.

3.5.3. Tissue Specific Down-Regulation by RNAi

After a recombination line between *UAS-CG4623RNAi* and *UAS-mitoGFP* was obtained as denoted in the previous section, the next step was to perform crosses to express these genes under ubiquitous, pan-neuronal and pan-glial GAL4 driver control. GAL4 lines were also crossed with *UAS-mitoGFP* line alone to be used as controls. Both crosses were kept at 25°C. Analyses of mitochondrial morphology were performed by immunohistochemistry and confocal microscopy. Crosses for this part are denoted in Figure 3.9.

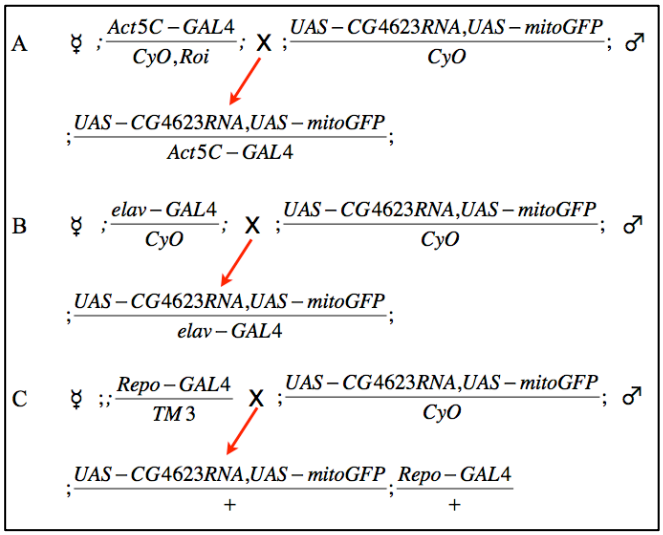

Figure 3.9. Crossing scheme for tissue-specific down-regulation of *CG4623* by RNAi. *CG4623* was down-regulated ubiquitously (A), in all neurons (B), and in all glia (C).

3.6. Targeting *CG4623* by Homologous Recombination

The HAs flanking the 5' and 3' of the *CG4623* gene were amplified with high fidelity PCR. They were cloned into the targeting vector pP{white-STAR} and then sent to Genetic Services Inc., USA for injection to the fly embryos. The host embryos used for injection of the target vector were of w^- background (white eye) carrying attP40 sites. Since pP{white-STAR} carries a red eye marker gene (w^+) between the homology arms, successful injection could be tracked by isolation of progeny flies red eyes.

The chromosomal location of the target vector integration site was mapped when the transformed flies were received. For this purpose, transgenic female flies having red eyes were crossed with quadruple-balancer male flies. Then, the homozygous lines for the IMAGO insertion were generated. In order for the homologous recombination event to take place, male homozygous IMAGO lines were crossed with virgin *hs:Flp, hs:ISce-I* flies, providing mobilization and linearization, respectively, upon heat-shock. The crosses were flipped every three days and the larvae at the stage of the second instar were exposed to heat-shock at 38ºC for 1 hour.

3.7. Histological Methods

3.7.1. Eye Imaginal Disc Dissection

Wandering third instar larvae from RNAi and control crosses were selected according to the presence of a GFP signal under a flourescence microscope. Dissections were performed within 30 min in order to avoid any harm to the tissue. Several drops of ice-cold 1X PBS were put onto silicone plates and then larvae were placed into PBS drops one by one. Afterwards, larvae were hold at the mouth hook on the anterior part using the forceps with a fine tip. Larvae were pulled from the middle part slowly with the help of another forceps. The complex containing the eye imaginal discs, two brain lobes and the VNC were pulled out and any undesired parts such as intestines and other imaginal discs were removed.

3.7.2. Immunohistochemistry for Eye Imaginal Disc Complex

The dissected complexes were placed into ice-cold 1X PBS in glass chambers and then fixed in 4% PFA for 20 min on a shaker set to 100 rpm. They were washed three times with PBX3 for 10 min each; then they were blocked with PAXDG solution for two hours. Selected primary antibodies were prepared in PAXDG solution and added into wells. After the glass chamber was closed with microscope slide and sealed with parafilm, it was placed on the shaker, which was set to 100 rpm, in the cold room and incubated overnight. On the next day, they were washed three times with PBX3 and then washing solution was replaced with secondary antibodies containing PAXDG. The glass chamber was covered with aluminum foil and incubated for two hours at room temperature. Then, it was washed again three times with PBX3 and then the dissected complexes were placed on a silicone plate and the two eye imaginal discs were separated from the complex. Both imaginal eye discs and the remaining two lobes with VNC were mounted on positively charged slides.

3.8. Analysis of Mitochondrial Morphology

After eye imaginal disc dissection and immunohistochemistry have been performed, they were further analyzed with confocal microscopy. In addition, mitochondrial morphology were analyzed in the eye imaginal disc in which *CG4623* was down-regulated in all neurons, glia or ubiquitously.

3.8.1. Confocal Microscopy

The eye imaginal discs were analyzed using Leica TCS SP5 confocal microscope. Eye imaginal discs were observed with 20X and 63X objectives. Further details for taking images are stated in Table 3.9. Images taken with 63X objective were used for the analyses of mitochondrial morphology while images taken with 20X objective were used to observe morphology of the eye imaginal disc.

Table 3.9. Optimized parameters used in confocal microscopy.

Objective	Digital Zoom	Line Average	Frame Average	Stack Thickness
20X	1.5	1	2	1.51 μm
63X	1	1	1	0.59 μm

3.8.2. Analysis of Mitochondrial Morphology using ImageJ Plug-in

Eye imaginal disc dissection and confocal microscopy parameters were optimized for the analysis of mitochondrial morphology. After obtaining optimal images, eye imaginal discs were analyzed for ubiquitous, pan-neuronal and pan-glial down-regulation of *CG4623*. For ubiquitous down-regulation seven eye imaginal discs were analyzed while nine eye imaginal discs were observed for pan-neuronal and another nine were observed for pan-glial down-regulation.

ImageJ software plug-in, namely Mitochondrial Morphology Analyses, was used to analyze mitochondrial network dynamics. For this purpose, the maximum projection of z-stacks of images was taken and then color channels were separated. Green channel, which is corresponding to GFP signal, was used for analysis but another channel was selected for determination of the area at which mitochondrial morphology analyses were performed. Afterwards, the green channel for each cross was auto-thresholded two times. At this point, mitochondria were shown as black pixels and they were analyzed using ImageJ plug-in. This software provides several parameters for the analyses, which are listed below; however, only elongation index, the inverse of circularity, was used in this study.

- Cell Count
- Total Area of Mitochondria
- Cellular Area
- Mitochondria Content
- Perimeters of Mitochondria
- Circularity of Mitochondria
- Average Perimeter
- Average Area
- Average Circularity

- Area/Perimeter
- Area/Perimeter normalized to minor axis
- Minor Axis
- Area/Perimeter normalized to circularity

3.8.3. Statistical Analyses of Mitochondrial Morphology

For statistical analyses, the averages and the standard deviations of the elongation index of each experiment were calculated. The P-value was calculated using a two-tailed t-test to determine if there is a significant difference between RNAi and control experiments.

3.9. Molecular Biology Techniques

3.9.1. Isolation of BAC DNA

Bacteria carrying the bacterial artificial chromosome (BAC), BACR12G07, containing the *CG4623* gene and large flanking regions, was purchased from BACPAC CHORI (USA). With the help of a sterile pipette tip, it was streaked onto an agar plate supplemented with 12.5 µg/ml chloramphenicol. After overnight incubation at 37°C, five single colonies were chosen randomly, inoculated into 5 ml of LB culture and grown overnight.

The next day the BAC DNA was isolated using GeneJET Plasmid Miniprep Kit solutions (Thermo Scientific). The overnight cultures were centrifuged at 3500 rpm for 10 min, and then supernatant was discarded. The pellet was resuspended in 750 µl of resuspension solution (P1) and then 750 µl of lysis solution (P2) was added and mixed by shaking gently. The suspension was left at room temperature for 5 min. Neutralization solution (P3) of 750 µl was added slowly; the tube was shaken gently, and left on ice for 5 min. Afterwards, the solution was centrifuged at 10000 rpm for 15 min at 4°C in Beckmann JA-14 rotor. The tube was left on ice for 10 min. Supernatant was transferred to a new tube containing 0.8 ml of cold isopropanol, and centrifuged at 13000 rpm for 15 min at 4ºC. After removal of the supernatant, the pellet was washed with 0.5 ml of 70 % ethanol and air-dried for 30 min. Then, the DNA was resuspended in 50 µl elution buffer.

3.9.2. Isolation of Plasmids

Plasmids were isolated using GeneJET Plasmid Miniprep Kit (Thermo Scientific) according to the manufacturer's instructions. All the centrifugation steps were performed at 14000 rpm and at room temperature, unless stated otherwise. Bacteria from a single colony were grown overnight in 5 ml LB medium supplemented with 100 µg/ml ampicillin. Cells were harvested at 8000 rpm for 2 min and then resuspended in 250 µl of P1 solution. After 250 µl of P2 solution was added, the solution was mixed by inverting the tubes gently and incubated for 5 min at room temperature. Afterwards, 350 µl of P3 solution was added and the tubes were mixed gently. After centrifugation for 5 min, the supernatant of each tube was transferred to a spin column of the kit. The columns were centrifuged for 1 min for binding of DNA and then the flow-through was discarded. The columns were washed with 500 µl wash solution and then centrifuged for 1 min. This step was repeated twice. In the last step, 50 µl of elution buffer was added to each tube and left at room temperature for 2 min and then centrifuged for 2 min. The flow-through was collected from each tube and their concentration was measured using NanoDrop spectrophotometer.

3.9.3. Preparation of Rubidium Chloride Competent Cells

Escherichia coli (*E. coli*) TOP10 cells were streaked on a nonselective LB agar plate. The next day, a single colony was inoculated into a starter culture of 20 ml SOC medium in a 125 ml flask. Then the culture was incubated overnight at 37 °C on a shaker, which was set to 200 rpm. From this starter culture, 2.5 ml was taken into 250 ml of 2X YT media in a 1 L flask. The culture was incubated at 37°C on a shaker until the OD600 value reached 0.4 to 0.6. Then the culture was taken on ice and bacteria were spun down at 4°C with a speed of 5000 g for 10 min. The supernatant was removed and the flask was rinsed gently with transformation buffer 1 (TFB1) to remove all medium. 100 ml TFB1 was added to the pellet for every 250 ml growth culture and the pellet was resuspended with a 10 ml serological pipette. After incubating on ice for 5 min, the resuspension was spun down at 4°C with a speed of 5000 g for 5 min. All of the supernatant was removed and 10 ml transformation buffer 2 (TFB2) was added. The pellet was resuspended with a serological pipette. After incubating on ice for half an hour, the prepared competent cells

were aliquoted into prechilled 1.5 ml centrifuge tubes and snap frozen in liquid nitrogen to be stored at -80°C.

3.9.4. Transformation of Bacteria

Rubidium chloride (RbCl) competent *Escherichia coli* (*E. coli*) TOP10 were thawed on ice. After 2 µl of ligation product was added and mixed gently, they were left on ice for 30 min. Then they were heat shocked for 90 seconds at 42ºC in water bath. Tubes were transferred to ice immediately for 2 min. Five hundred µl of LB medium was added and then they were incubated in a shaker at 37°C for one hour. Different volumes of recovery culture, ranging from 20 µl to 100 µl, of each transformation product were spread onto selective agar plates and incubated at 37ºC overnight. On the next day, colonies were picked for further analysis.

3.9.5. Restriction Digestion

Digestion of BAC or plasmid DNA was performed using 1 µg of target DNA and 10 units of the relevant restriction enzyme in 50 µl of reaction mix for one hour at 37 ºC. The restriction fragments were analyzed on the agarose gel. If it was necessary, the band of interest was extracted from the gel.

3.9.6. Ligation of DNA Fragments

The amplified DNA fragments were ligated either into pGEM-T Easy Vector or targeting vector pP{white-STAR}. For pGEM-T Easy ligations, A-tailed DNA fragments were added into ligation reaction solution at molar ratios of 1:1 or 1:3 and incubated at 4°C. On the other hand, T4 DNA ligase was used for ligation to targeting vector pP{white-STAR}. Targeting vector and DNA fragments digested with relevant restriction enzymes, were added to the reaction solution with a molar ratio of 1:3, and incubated for 1 hour at 22°C. After ligation, they were transformed into RbCl treated competent cells.

3.9.7. High Fidelity PCR

The 5’ and 3’ HA flanking *CG4623* were amplified using BACR12G07 as a template. For this purpose, two primer pairs were designed having restriction sites. In order to amplify 5’ HA, CG4623_5HF and CG4623_5HR primers were designed that had *Kpn*I and *Avr*II restriction sites, respectively. To amplify the 3’ HA CG4623_3HF and CG4623_3HR primers having *Nhe*I and *Sac*II restriction sites were designed, Phusion High-Fidelity DNA Polymerase was used and the amplification conditions were adapted to match the properties of the designed primers. High Fidelity PCR mixture and PCR cycles used for this purpose are given in the Table 3.10 and Table 3.11, respectively. The presence of desired fragments were analyzed by loading 5 µl of each reaction and 1 µl of agarose loading buffer on a 1% TAE agarose gel. Upon confirmation, the rest of the reactions were loaded into a single well in order to purify the desired fragment by gel extraction.

Table 3.10. PCR mixture contents used for high fidelity PCR.

Reagents	
Template DNA	2 µl
High Fidelity Buffer (1X Final concentration)	10 µl
10 mM dNTP	1 µl
Forward Primer	2.5 µl
Reverse Primer	2.5 µl
Phusion High-Fidelity DNA Polymerase	0.5 µl
dH_2O	31.5 µl
Total	50 µl

Table 3.11. High fidelity PCR cycle conditions.

Temperature	Time	Number of Cycle(s)
98°C	30”	1
98°C	30”	35
68°C for 5’ HA 61.8°C for 3’ HA	20”	
72°C	1’	
72°C	10’	1

3.9.8. Colony PCR

Colonies were selected from the agar plate on the next day of the transformation experiment and colony PCR was performed to verify the success of the transformation reaction. By using a sterile pipette tip, colonies were picked and dipped into a sterile H_2O-containing PCR tube. Then, 5 µl of this solution was put into the colony PCR reaction solution. The colony PCR mixture content and PCR cycle used in this study are stated in the Table 3.12 and Table 3.13. The success of the amplification was assessed by loading 5 µl of each reaction product with 1 µl of agarose loading buffer on a 1% TAE agarose gel and visualized under UV light.

Table 3.12. PCR mixture used for the colony PCR.

Reagents	
Template DNA	2 µl
Taq Buffer with $(NH_4)_2SO_4$	2.5 µl
$MgCl_2$	2 µl
10 mM dNTP	0.5 µl
Forward Primer	1 µl
Reverse Primer	1 µl
Taq DNA Polymerase	5 µl
dH_2O	16.5 µl
Total	30 µl

3.13. Colony PCR cycle conditions.

Temperature	**Time**	**Number of Cycle(s)**
95°C	5’	1
95°C	45”	35
60°C for 5’ HA 61.4°C for 3’ HA	45”	
72°C	1’	
72°C	10’	1

3.9.9. Gel Extraction of DNA

After confirming the presence of the desired DNA fragment in the colony, the DNA fragment was isolated from the agarose gel. For this purpose, pooled PCR or restriction digestion reactions were loaded on a 1% TAE agarose gel. Then the agarose gel was analyzed under UV illumination and if the size of the band was correct, it was cut from the gel and put into a sterile tube. Agarose Gel Extraction Kit (Roche) was used for further isolation and purification.

4. RESULTS

In our laboratory we aim to elucidate the function of GDAP1 and find out how *GDAP1* mutations associated with CMT may cause the disease phenotype. The generation of the loss of function phenotypes is the best way to understand and gain some information about the protein. Loss of function studies can be done by various methods, but in this study we used the homologous recombination technique to knockout the fly homolog of *GDAP1*, *CG4623,* and RNAi method to down-regulate the expression of this gene. To knockout the gene of interest, the IMAGO technique was used. This technique is advantageous as it provides the ability to knock-in wild type and mutant forms of *GDAP1* using RMCE. On the other hand, RNAi lines contain 300-400 bp inverted repeats specific to the 3' UTR of *CG4623* and are under UAS control, therefore inactivate the gene if the genotype also includes a GAL4 driver. Since the gene can be expressed spatially and temporally with the help of GAL4 drivers, the function of *CG4623* can be studied in different tissues and at different developmental stages.

4.1. Loss of Function Experiments: RNAi

4.1.1. Determination of Down-regulation Levels in the Ubiquitously Down-regulated RNAi Lines

The quantitative RT-PCR method was used to confirm the down-regulation of *CG4623*. For this purpose, *UAS-CG4623RNAi line*, purchased from VDRC, were crossed with *Act5C-GAL4* to ubiquitously down-regulate *CG4623.* As a control, progeny flies of a cross between *Act5C-GAL4* and w^{1118} were used. Total RNA was isolated from 30 flies with the genotype *; UAS-CG4623RNAi/Act5C-GAL4;* and w^{1118}*; Act5C/+;*. An equal number of 5-week-old male and female flies were collected and qRT-PCR experiment was performed to confirm down-regulation of *CG4623.*

The comparative threshold cycle was calculated and the *Actin79b* gene was used as the internal control. The CG4623_RT primer pair was designed to cover the first and second exon that harbors a large intron in-between to prevent any genomic DNA

contamination. The size of the expected PCR product was 159 bp for *CG4623*. The Actin79b_RT primer pair was chosen to be on the exon-exon boundary of the second and third exons to produce an amplification product of 167 bp in length. As the starting material for qPCR, RT product was used in equal amounts for each reaction without further processing or purification and this amount was the same for both Actin79b_RT and CG4623_RT primer pairs. Since these reactions were performed in the same run, this allowed use of the comparative threshold cycle method to approximate RNA level of *CG4623* compared to the level of *Actin79b*.

After isolation of total RNA and first-strand cDNA synthesis, the qRT-PCR was performed in triplicates for three different cDNA samples for both the RNAi line and the control flies. Using CG4623_RT and Actin79b_RT primer pairs, a total of nine samples were quantified in the same run. As it can be seen in Figure 4.1, the amplification curves drawn for all of the samples reveal a difference in pattern between *Actin79b* and *CG4623* products.

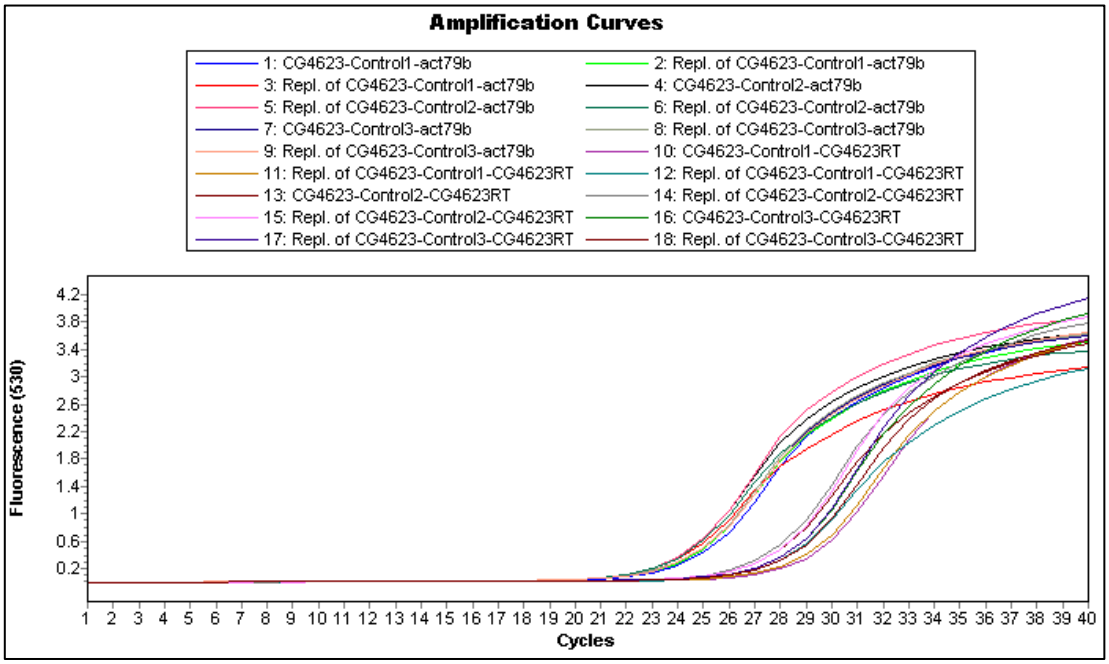

Figure 4.1. Amplification curves for control lines. All of the samples with their replicates are represented.

In order to ensure that the results were not affected by mispriming or genomic DNA amplification, melting curve analysis was performed (Figure 4.2). As there are only

two peaks, focusing on 83°C and 87°C, which correspond to *Actin79b* and *CG4623* products, respectively, it was shown that non-specific products were not amplified at a noticeable level. The threshold cycles and standard deviations of each triplicate were calculated using the LightCycler software for which the results can be found in Table 4.1. The average threshold cycle was calculated to be 22.86 for *Actin79b* and 26.82 for *CG4623*. The difference of 3.96 cycles between the two showed that *CG4623* was expressed at a level of 6.41% of *Actin79b* in the control flies, where RNAi was not activated.

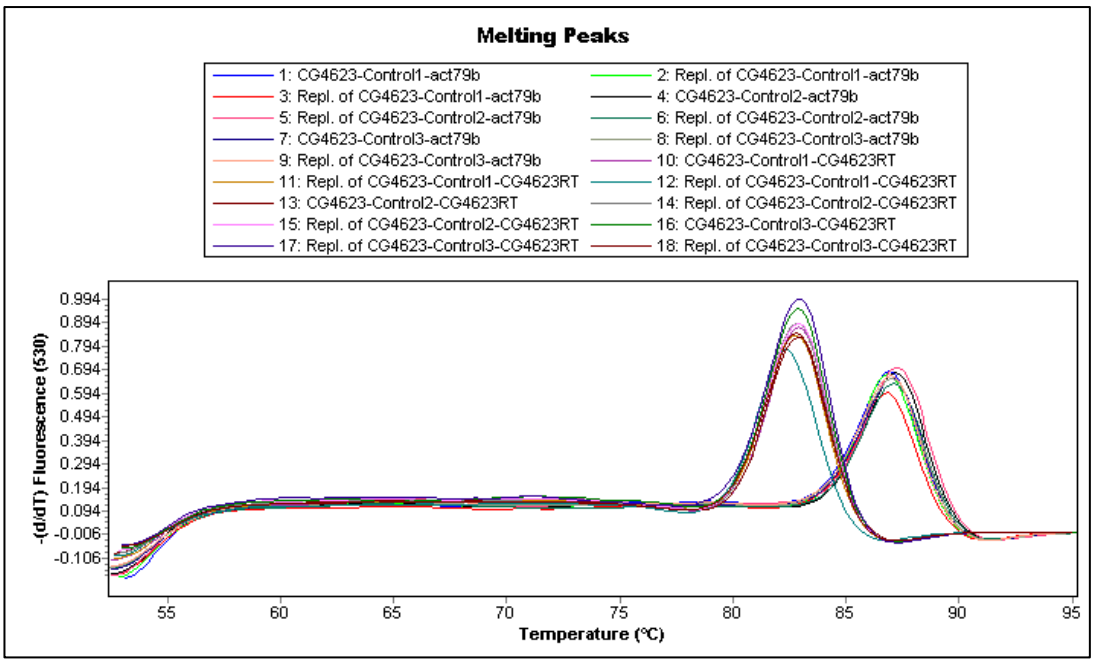

Figure 4.2. Melting curve for control lines. The two peaks correspond to melting temperatures of PCR products using Actin79b and CG4623 primers.

After quantifying the RNA levels of *CG4623* and *Actin79b* in control flies, the same procedure was applied to the progeny of the crosses that had RNAi activated ubiquitously using the *Act5c-GAL4* driver. For these *CG4623* down-regulated flies, the amplification curves were drawn for each sample (Figure 4.3). It can be seen that nine different trend lines for each primer pair grouped among themselves closely.

In order to verify that the amplification was specific, melting curve analysis was performed (Figure 4.4). The melting curves peaked at two different locations, at 83°C and 87°C, which correspond to *Actin79b* and *CG4623* products, respectively, showing that the

intended fragments were amplified. The threshold cycles and standard deviations of each triplicate calculated using the LightCycler software could be found in Table 4.1. As the average threshold cycle was calculated to be 20.53 for *Actin79b* and 27.58 for *CG4623*, the difference of 7.07 cycles between the two showed that *CG4623* was expressed at a level of 0.74% of *Actin79b* in the RNAi flies, where *CG4623* was down-regulated.

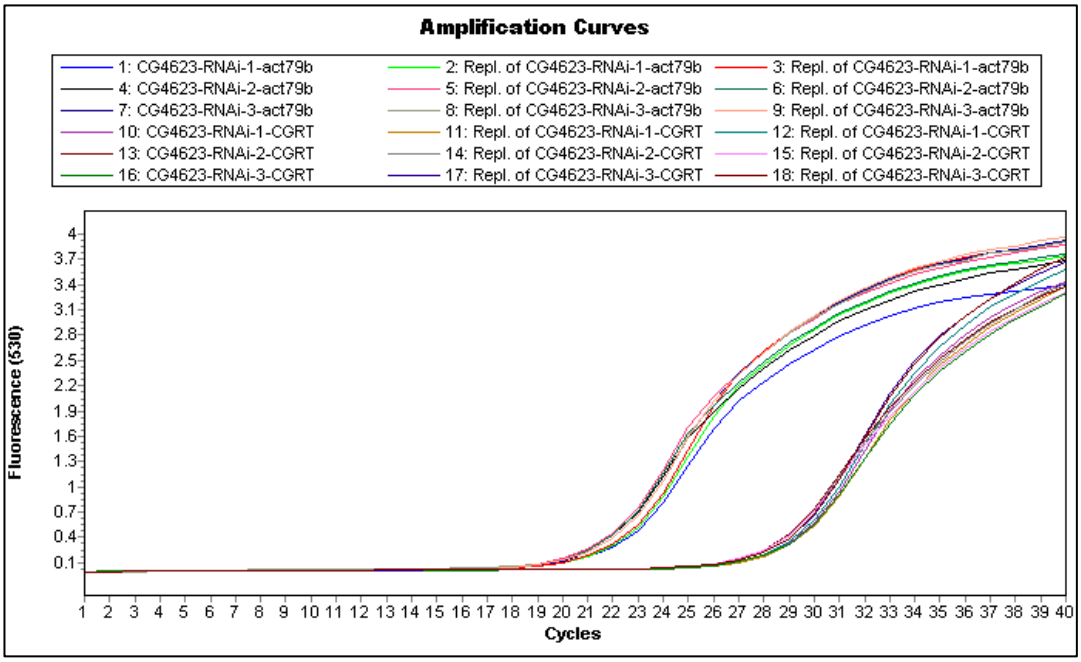

Figure 4.3. Amplification curves for RNAi lines. All of the samples with their replicates are represented.

In this study, the same pairs of primers (*CG4623* and *Actin79b*) were used to amplify equal amounts of first-strand synthesis product after reverse transcription. Therefore *CG4623* levels between samples can be compared by normalization to *Actin79b* as the housekeeping gene. Direct comparison between *Actin79b* levels among control crosses and RNAi crosses was not possible since the starting cDNA amount cannot be quantified when the RT product is directly used without purification, as in this case. However, as *Actin79b* is a ubiquitously expressed gene and variance is small among flies with the same genotype, it can be used to normalize the levels of *CG4623* in different samples. Therefore, *CG4623* mRNA level was approximated to be 6.41% of *Actin79b* levels in control flies. In RNAi flies, *CG4623* mRNA level was observed to be 0.74% of *Actin79b* mRNA levels. As a result, it was determined that *CG4623* mRNA levels were lowered by 88.4% in RNAi lines compared to the control.

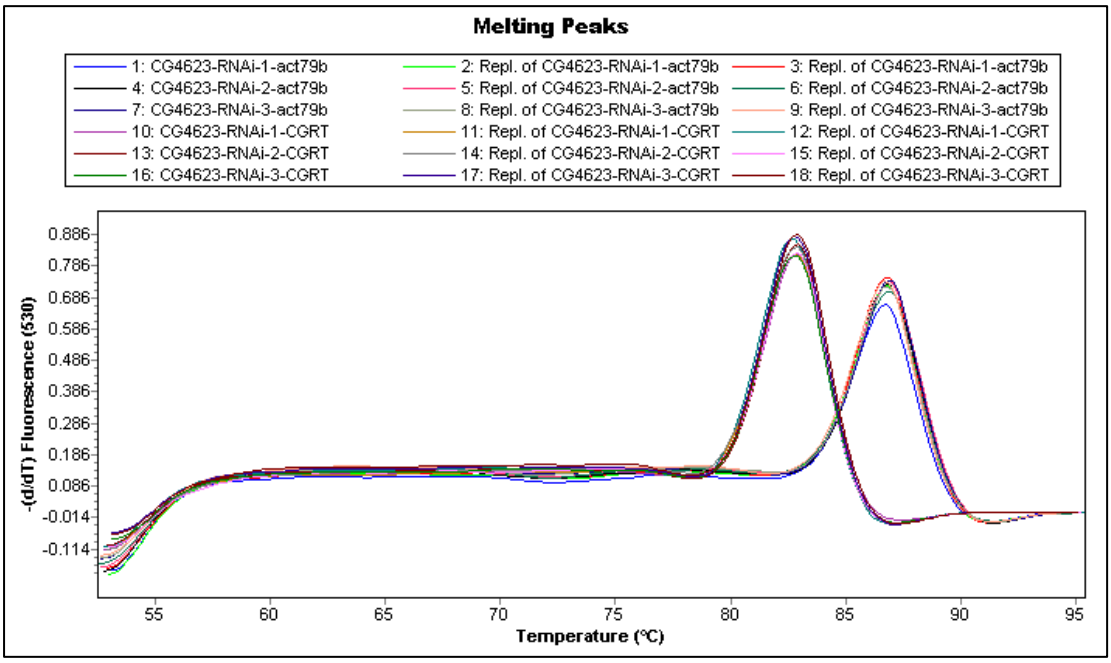

Figure 4.4. Melting curve for RNAi lines. The two peaks correspond to melting temperatures of PCR products using Actin79b and CG4623 primers.

Table 4.1. The comparative analysis of the expression levels of *CG4623* in control and RNAi lines using qRT-PCR.

Control				**RNAi**			
Experiments	**Samples**	**Average CT**	**STD CT**	**Experiments**	**Samples**	**Average CT**	**STD CT**
1. Actin79b	1, 2, 3	22.9	0.41	**1. Actin79b**	1, 2, 3	20.88	0.03
2. Actin79b	4, 5, 6	22.66	0.11	**2. Actin79b**	4, 5, 6	20.13	0.02
3. Actin79b	7, 8, 9	23.02	0.02	**3. Actin79b**	7, 8, 9	20.53	0.01
Average		22.86	0.18	**Average**		20.53	0.02
1. CG4623	10, 11, 12	27.34	0.64	**1. CG4623**	10, 11, 12	27.84	0.04
2. CG4623	13, 14, 15	26.22	0.2	**2. CG4623**	13, 14, 15	27.2	0.03
3. CG4623	16, 17, 18	26.91	0.08	**3. CG4623**	16, 17, 18	27.71	0.05
Average		26.82	0.31	**Average**		27.58	0.04
Cycle Difference		3.96		**Cycle Difference**		7.07	
Level Difference		$2^{3.96}$		**Level Difference**		$2^{7.07}$	
CG4623 expression level normalized to Actin79b		6.41%		**CG4623 expression level normalized to Actin79b**		0.74%	
The level of CG4623 (RNAi/Control line)						11.6%	
The percentage decrease in the expression of *CG4623* (RNAi/Control line)						**88.4%**	

4.1.2. Tissue Specific Down-regulation of *CG4623*

In order to analyze how down-regulation of *CG4623* affects mitochondrial morphology in the fly, we made use of a reporter line in which GFP is expressed with a mitochondrial import signal, *UAS-mitoGFP*. This reporter line was crossed with *CG4623*RNAi lines in which *CG4623* was down-regulated using different drivers. As the *UAS-CG4623* and *UAS-mitoGFP* are on the 2nd chromosome, flies that have both genes in cis on the same chromosome were needed for further analyses. Thus, *UAS-mitoGFP* mitochondrial import signal gene was recombined with *CG4623*RNAi gene to segregate together in further crosses. These flies are expected to allow observation of changes in mitochondrial morphology in tissues in which *CG4623* is down-regulated. Controlled expression was achieved in neurons and glia as well as ubiquitously using *elav-GAL4*, *repo-GAL4*, and *Act5C-GAL4* lines for the crosses, respectively. To analyze the mitochondrial morphology upon down-regulation, the eye imaginal disc of the fly was used as a model.

Mitochondrial morphology has not been studied previously in our department; thus, we had to optimize a methodology for the observation and analysis of mitochondria. For this purpose, different eye imaginal disc dissection techniques were tested to optimize the technique and to obtain as many eye imaginal discs as possible in a limited time period. Afterwards, immunohistochemistry experiments were performed in order to visualize mitochondria and other subcellular structures or different cell types with various antibodies, which are listed and explained in Table 4.2. Antibodies were tested at different concentrations in immunohistochemistry to obtain clear images that would allow processing and analysis. After dissection and immunohistochemistry, imaginal discs were visualized by taking images using confocal microscopy. Images were generated using different objectives and different stack thicknesses. In addition, line and frame averages were optimized to get a clear image. While performing these optimizations, fly stocks to analyze mitochondrial morphology in the eye imaginal disc in which *CG4623* was down-regulated in all neurons, glia or ubiquitously were prepared.

Table 4.2. Antibodies used in this study and their targets in the cell.

Antibody	Target	Used Color
Elav	Nuclei of neurons	Alexa647 (Blue)
Repo	Nuclei of glia	Alexa555 (Red)
GFP	GFP on mitochondria	Alexa488 (Green)

The initial experiments were the ubiquitous down-regulation of *CG4623*. *Act5C-GAL4* virgin female flies were crossed with male *UAS-CG4623RNAi, UAS-mitoGFP* flies and the vials were kept at 25°C. In addition, we used the progeny of the cross between *Act5C-GAL4* and *UAS-mitoGFP* as the control. After few days, wandering third instar larvae with the desired genotype were selected using fluorescence microscopy for detection of the GFP signal. Then eye imaginal disc dissection was performed to analyze mitochondrial morphology. Dissected eye imaginal discs were immunostained with anti-GFP, anti-repo, and anti-elav antibodies. Successfully immunostained eye imaginal discs were analyzed with confocal microscopy. We expected to observe green GFP signals throughout the eye imaginal disc since *Act5c* is expressed ubiquitously. The expectation was that more elongated mitochondria are observed in RNAi experiments since *GDAP1* (and thus its fly homolog *CG4623*) is thought to be the regulator of mitochondrial fission events. On the other hand, control experiments should result in the observation of homogenously distributed tubular and circular mitochondria in the eye imaginal disc. A slightly larger elongation index for mitochondria was observed for the RNAi line as compared to control samples. The images were analyzed using Mitochondrial Morphology, an ImageJ plug-in. The results however appeared not to be significant when tested with the two-tailed t-test and gave a p-value of 0.54 (Figure 4.5; Table 4.3).

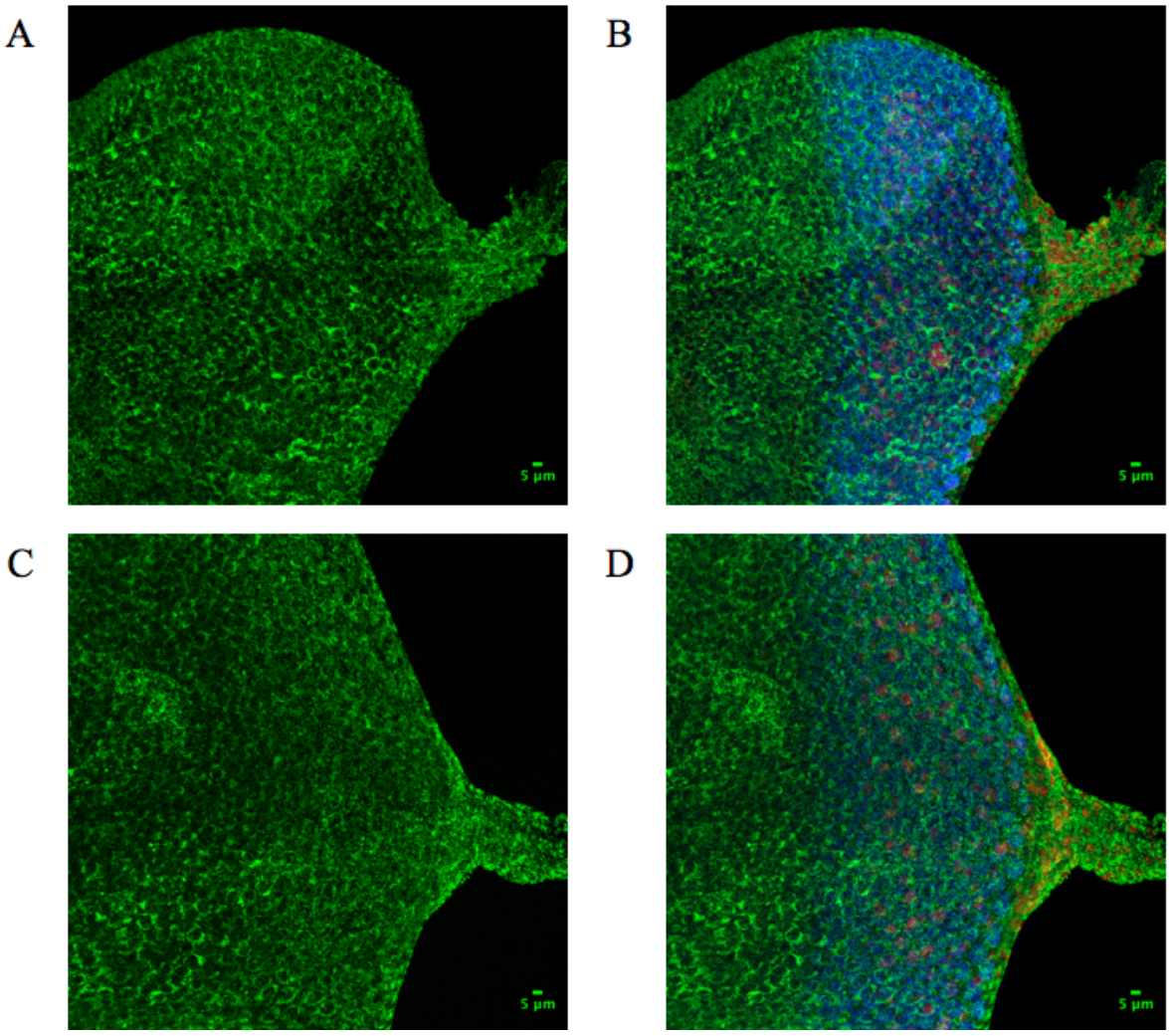

Figure 4.5. Mitochondrial morphology of the eye imaginal discs in control and *CG4623* ubiquitous down-regulation larvae. The images were obtained using a 63X objective of the confocal microscope. Control larvae of genotype *Act5C-GAL4 > UAS-mitoGFP* (A and B) and *Act5C-GAL4 > UAS-CG4623RNAi, UAS-mitoGFP* (C and D) were successfully stained with antibodies against GFP (green), Repo (red) and Elav (blue).

Table 4.3. Average elongation indices of ubiquitous down-regulation of *CG4623* and control larvae.

	Average	**Standard Deviation**
RNAi	0.184094198	0.115696287
Control	0.153090876	0.063649116

Even though we could not observe a significant change between RNAi and control discs, we optimized the technique to observe mitochondria within the eye imaginal discs. Furthermore, we suspected that overall down-regulation might have induced a neutralizing effect. In other words, the effect of tissue-specific decrease on mitochondrial dynamics could have been overcome through a secondary mechanism. As the interaction between neurons and Schwann cells in humans dictate pathogenic mechanism in many CMT cases, we wanted to observe the effect of down-regulation only in neurons or only in glia to see how cell specific down-regulation would affect the phenotype.

In a second set of experiments, *CG4623* was down-regulated using the pan-neuronal driver *elav-GAL4*. The third instar eye imaginal discs of experimental and control larvae were stained with anti-GFP and anti-Elav antibodies and analyzed as in the previous experiment (Figure 4.6). When we compared the elongation indices for each genotype, we observed again a slight increase; however, it was not significant according to the two-tailed p-value, which was 0.2591 (Table 4.4).

GDAP1 is known to be expressed in both axons and myelinating Schwann cells. Thus, *CG4623* was down-regulated in glia using the *repo-GAL4* driver to assess the possible contribution of glia to the phenotype. Afterwards, mitochondrial morphology of the larvae from control and RNAi crosses was examined using anti-GFP and anti-Repo antibodies and quantified as in the previous experiments (Figure 4.7). We calculated and compared the average elongation index and performed statistical analysis; however, no significant difference was observed since the two-tailed p-value was 0.21 (Table 4.5).

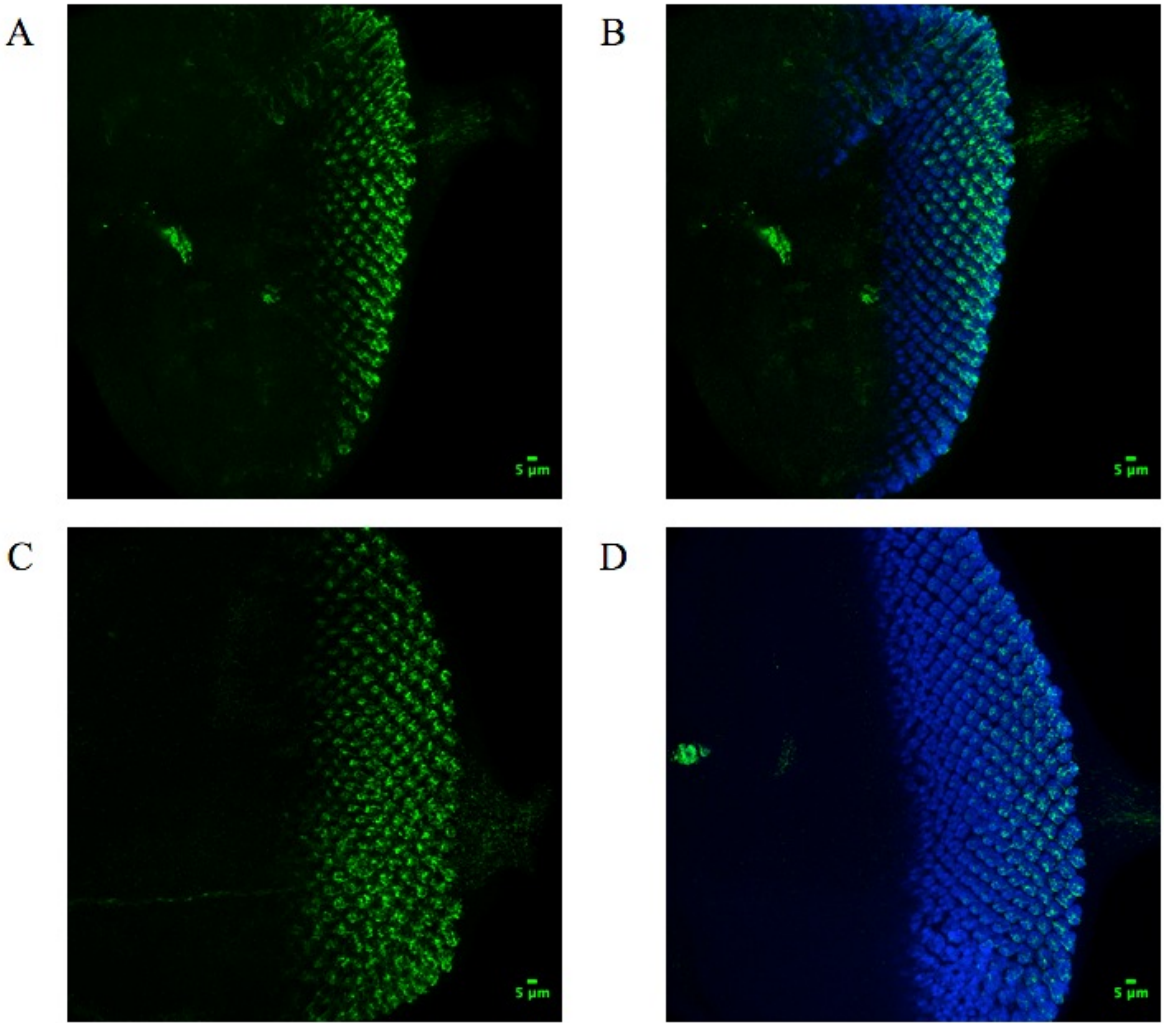

Figure 4.6. Mitochondrial morphology of the eye imaginal discs in control and *CG4623* panneuronal down-regulation larvae. The images were obtained using a 63X objective of the confocal microscope. Control larvae of the genotype *elav-GAL4 > UAS-mitoGFP* (A and B) and *elav-GAL4 > UAS-CG4623RNAi, UAS-mitoGFP* (C and D) were successfully stained with antibodies against GFP (green) and Elav (blue).

Table 4.4. Average Elongation indices of panneuronal down-regulation and control larvae.

	Average	**Standard Deviation**
RNAi	0.150272098	0.052589114
Control	0.12295015	0.046355905

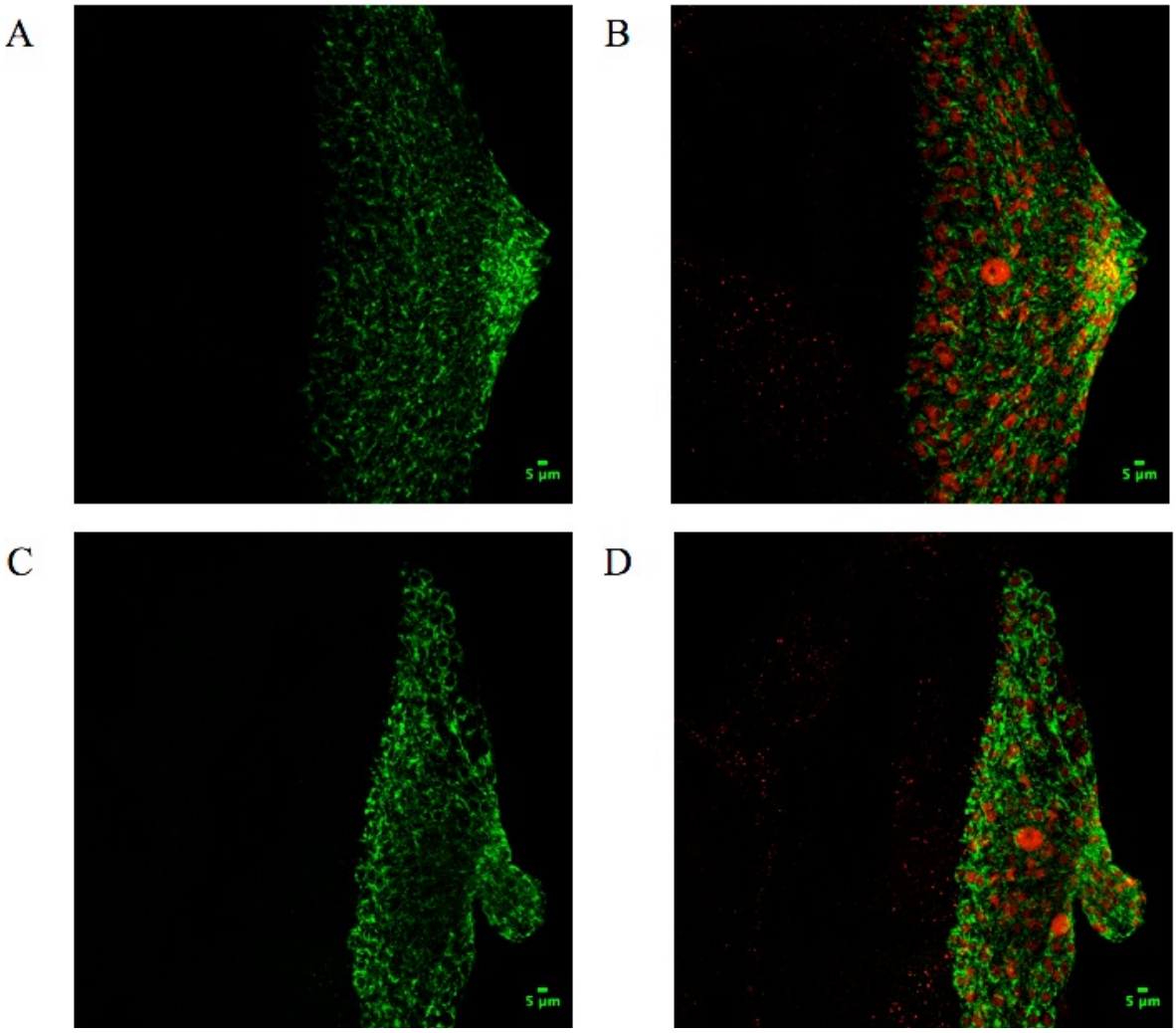

Figure 4.7. Mitochondrial morphology of the eye imaginal discs in control and *CG4623* panglial down-regulation larvae. The images were obtained using a 63X objective of the confocal microscope. Control larvae of the genotype *repo-GAL4 > UAS-mitoGFP* (A and B) and *repo-GAL4 > UAS-CG4623RNAi, UAS-mitoGFP* (C and D) were successfully stained with antibodies against GFP (green) and Repo (red).

Table 4.5. Average Elongation indices of panglial down-regulation and control larvae.

	Average	**Standard Deviation**
RNAi	0.097442659	0.047172649
Control	0.076564526	0.011796982

In contrast to the results obtained in the larval eye, we observed significant morphological differences between RNAi and control larva when the nerve bundles projecting from the VNC were analyzed (Figure 4.8). While the control larvae included mitochondria of various sizes, the RNAi line displayed long tubular mitochondria, which are mostly absent in the controls in this dissection. It was also noted that the number of mitochondria was low in the RNAi line, suggesting defects in mitochondrial movement and fission. Although we observed an apparent difference between RNAi and control larvae, we could not quantify the experiment as we had only one larva for each experiment. This finding suggested that nerve bundles projecting from the VNC are a better model to study mitochondrial morphology since they present a less crowded cellular environment than that of eye imaginal discs and give clear images.

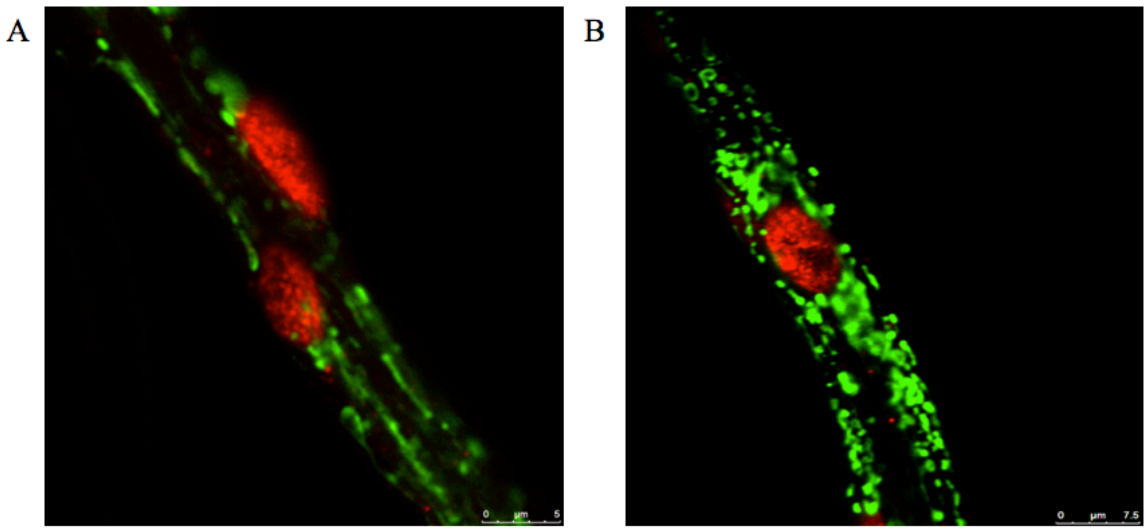

Figure 4.8. Mitochondrial morphology of the nerve bundles in control and *CG4623* panglial down-regulation larvae. The images were obtained using a 63X objective of the confocal microscope. Control larvae of the genotype *repo-GAL4 > UAS-mitoGFP* (A) and *repo-GAL4 > UAS-CG4623RNAi, UAS-mitoGFP* (B) were successfully stained with antibodies against GFP (green) and Repo (red).

4.2. Loss of Function Experiments: IMAGO

4.2.1. Generation of a *CG4623* Targeting Construct

The deletion of the *CG4623* gene in flies was one of the approaches used in this study to analyze the function of *CG4623* (Figure 4.9). Homologous recombination technique was used for this purpose as it generates precise knockout without interrupting any other region in the genome. For this purpose, a targeting construct for *CG4623* was prepared. The construct was prepared using pP{white-STAR} vector that carried two homology arms (HAs) flanking *CG4623* providing the necessary alignment capacity for the homologous recombination to take place. pP{white-STAR} contains a red eye marker (w^+); therefore, when the targeting vector is integrated into the genome of a fly with w^- background, the progeny can be selected by presence of a red eye color. In addition, the vector carries two FRT sites; I-*Sce*I restriction sites and two *attP* sequences. With the help of FRT sites, the integrated vector can be flipped out from the genome in the presence of a flippase, while I-*Sce*I sites are used to linearize the flipped out circular DNA. The final goal is that the linear fragment aligns with the targeted region and homologous recombination takes place, thereby exchanging *CG4623* with the white gene (w^+). At the same time *attP* sites flanking the white gene would be introduced to the endogenous gene locus. The importance of the *attP* sites is that they can later be used to exchange the white gene with any desired sequence flanked by *attB* sites using RMCE.

The length of pP{white-STAR} is 7237 bp and it carries two multiple cloning sites (MCS) flanking the marker gene. In this project, the modified version of this vector was used, in which two additional restriction sites, *Nhe*I and *Sac*II, were present (Kaçmaz G., 2013). *Kpn*I, *Avr*II, *Nhe*I and *Sac*II were used for cloning of the two homology arms into the pP{white-STAR}, 5' HA, and 3' HA respectively.

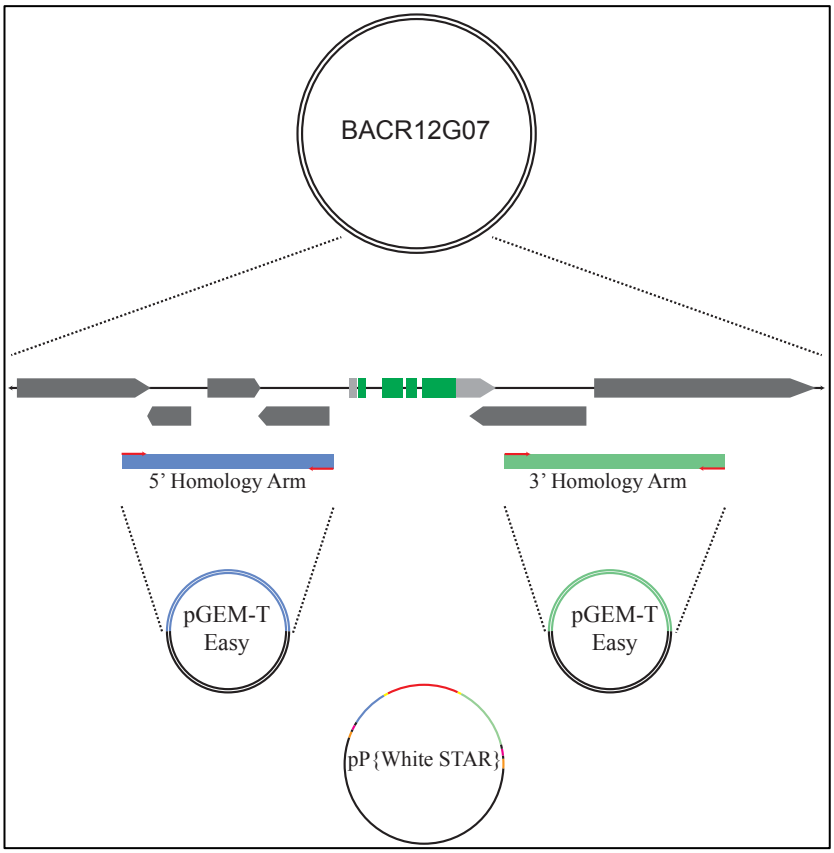

Figure 4.9. The strategy for targeting *CG4623* in this study.

4.2.1.1. Restriction digestion of BACR12G07 using *BamH*I restriction enzyme. The BAC clone BACR12G07 with a length of 180 kb, spanning *CG4623* and its flanking regions was purchased and cultured as described. BAC DNA was isolated from five selected colonies. The purchased BAC was verified by *BamH*I digestion (Figure 4.10). This digestion generates 28 bands, but as some DNA fragments were very close in length we could not observe them totally separated, though most of the expected distinct bands were observed, which confirmed that the clone was correct.

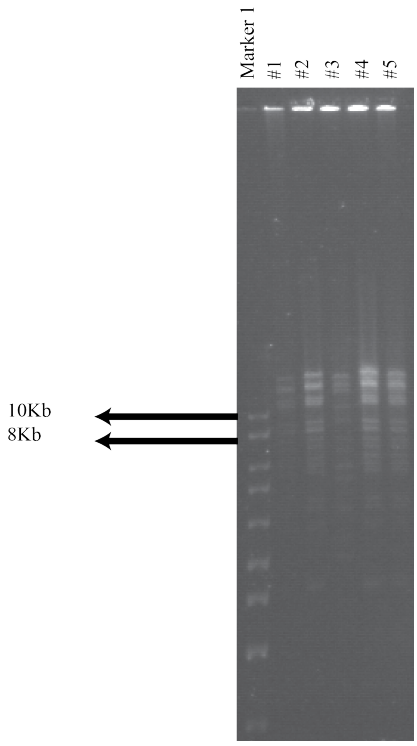

Figure 4.10. The BACR12G07 was validated by *BamHI* digestion.

4.2.1.2. Amplification of two HAs flanking *CG4623* using high fidelity PCR. In order to amplify 5' and 3' HAs, primers were designed according to the MCS of pP{white-STAR} with the help of Ape-A Plasmid Editor v2.0.38 (Figure 4.11). During the selection process, close melting temperature of primer pairs and lack of any nonspecific binding were used as criteria.

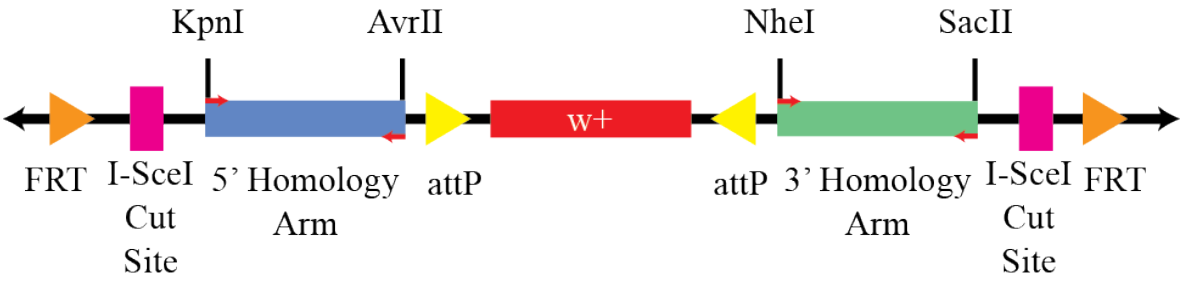

Figure 4.11. Targeting construct, pP{white-STAR} for *CG4623*. Primers having corresponding restriction sites were denoted with red arrows.

The 5' HA was amplified using primer pair CG4623_5HF and CG4623_5HR carrying *Kpn*I and *Avr*II restriction sites, respectively. On the other hand, primer pair CG4623_53F and CG4623_3HR was used to amplify the 3' HA carrying *Nhe*I and *Sac*II

restriction sites, respectively. The HAs flanking the 5' and 3' of the *CG4623* gene were amplified using Phusion High-Fidelity DNA polymerase with stated annealing temperatures. Expected DNA fragments of 3253 bp and 3385 bp, respectively, were observed after amplification (Figure 4.12). While the 5' HA was isolated from the gel and then cloned to the subcloning vector pGEM-T Easy, 3' HA was cloned directly using the PCR product (Figure 4.13).

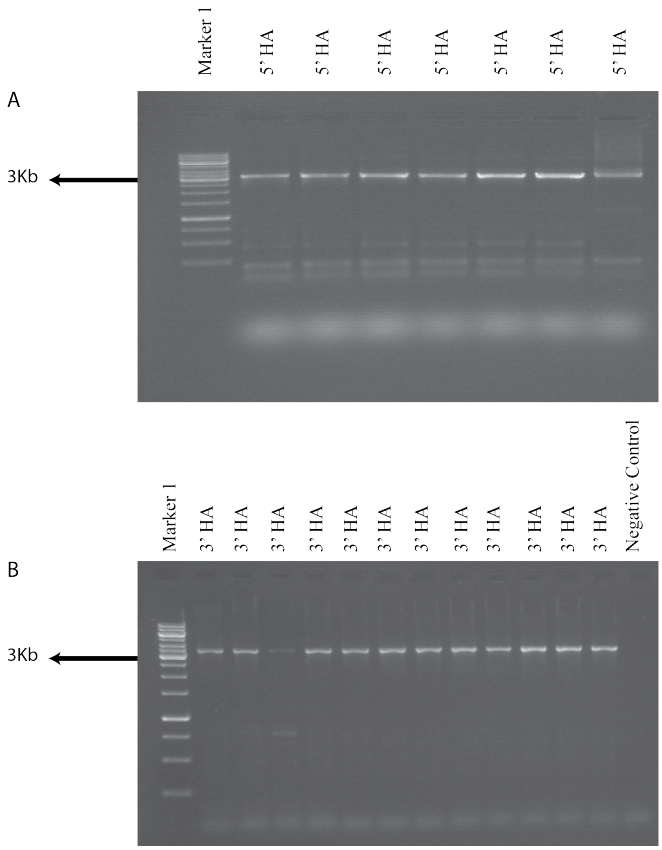

Figure 4.12. Amplification of 5' and 3' HAs flanking *CG4623* with high fidelity PCR. Marker 1 stands for 1kb DNA ladder (SM0311, Thermo Scientific). In part A, seven of the PCR products of 5' HA amplification were loaded to the gel, while 12 of the PCR products of 3' HA amplification were loaded in part B. All of them were positive and used in further experiments.

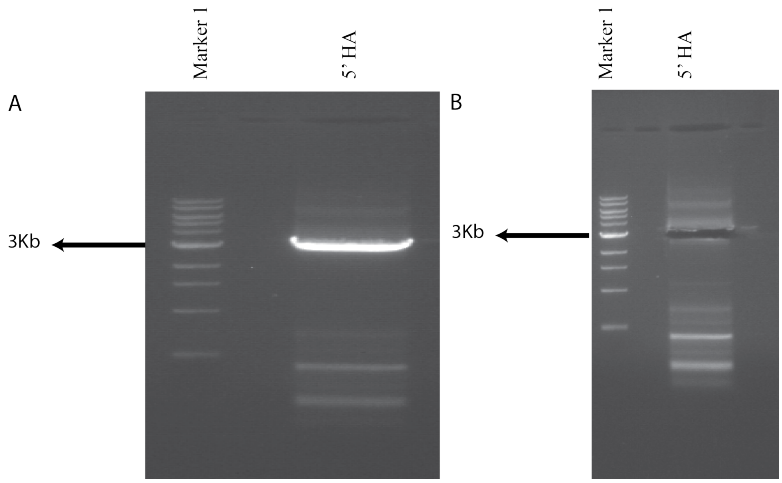

Figure 4.13. 5' HA was isolated from the gel successfully. Marker 1 stands for 1kb DNA ladder (SM0311, Thermo Scientific).

4.2.1.3. Cloning of 5' and 3' HAs into the pGEM-T Easy Vector. Amplified 5' and 3' HAs were subcloned into the pGEM-T Easy Vector, separately. As the vector has overhangs of a single T nucleotide in both ends, both HA amplicons were A-tailed. After performing ligation reactions for each HA, they were transformed into competent *E.coli* cells. The next day, colonies were picked and the presence of the ligation product with the desired insert was confirmed using colony PCR (Figure 4.14). For 5' HA, CG4623_5HS4 and CG4623_5HR primer pair was used in the colony PCR. An amplicon with a length of 878 bp for 5' HA was observed. On the other hand, a PCR product with a length of 1038 bp was observed using CG4623_3HS4 and CG4623_3HR for 3' HA. Colonies were picked for each HA (6, 7, 10, 11, and 12 for 5' HA and 2, 4, and 11 for 3' HA) and plasmids were isolated after overnight incubation of bacterial cultures. The next day, analytical digestion was performed for each HA using *EcoR*I (Figure 4.15). As *EcoR*I restriction sites are located on the backbone of pGEM-T Easy vector flanking the multiple cloning site, it releases the cloned fragment from the vector, creating fragments with the length of 3016 bp for pGEM-T Easy vector backbone along with 3253 bp for 5' HA and 3385 bp for 3' HA, which were observed as expected.

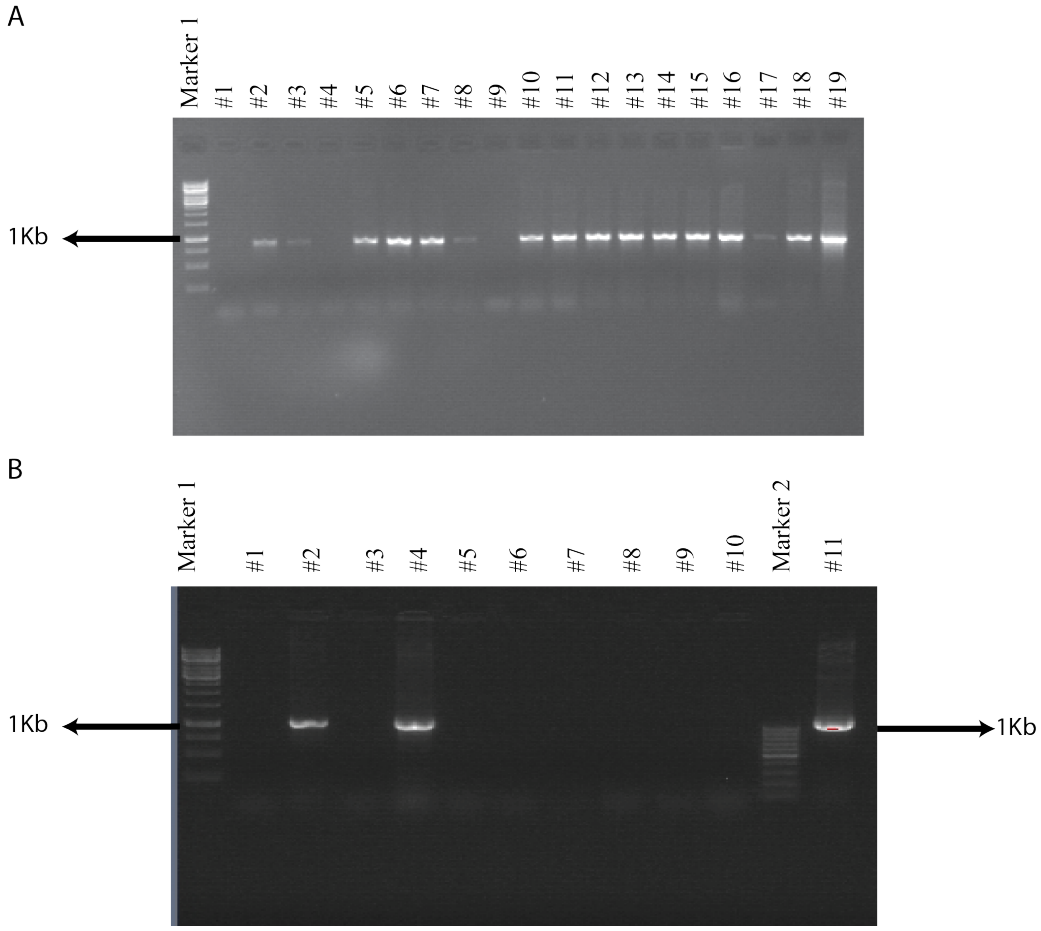

Figure 4.14. Verification of cloning of 5' HA (A) and 3' HA (B) into pGEM-T Easy vector. Marker 1 stands for 1kb DNA ladder and Marker 2 for 100bp ladder (SM0311 and SM0241, Thermo Scientific, respectively). Expected bands with a length of 878 bp (5' HA) and 1038 bp (3' HA) were obtained with colony PCR.

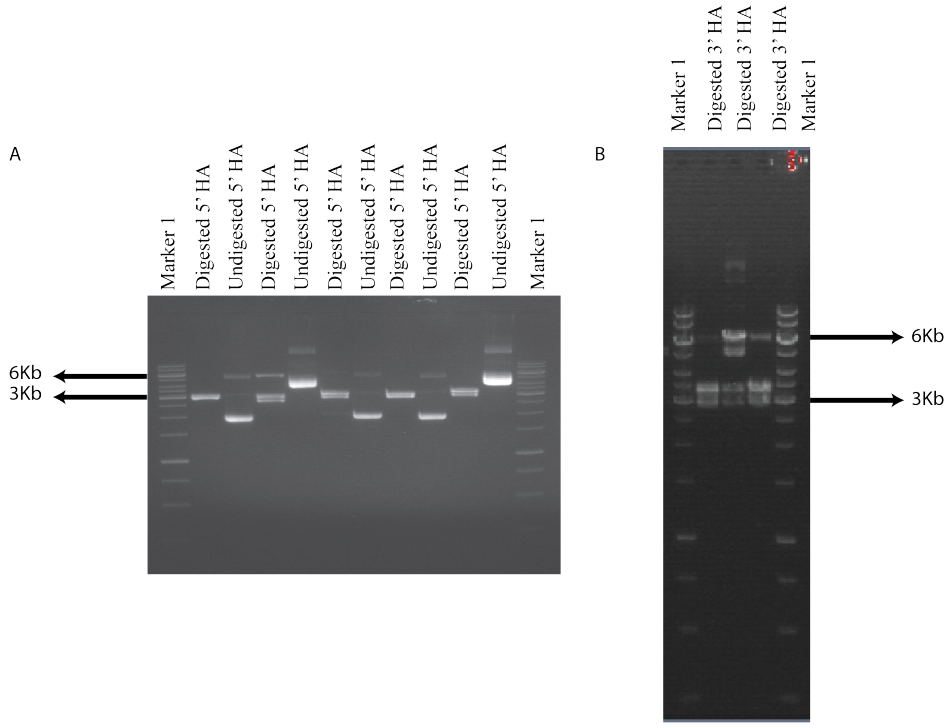

Figure 4.15. Analytic digestion of pGEM-T Easy vector containing 5' HA (A) and 3' HA (B) using *EcoR*I restriction enzyme. Marker 1 stands for 1kb DNA ladder (SM0311, Thermo Scientific). Both restriction digestions resulted in expected fragments with a length of 3016 bp (pGEM-T Easy Vector), 3253 bp (5' HA) and 3385 bp (3' HA).

4.2.1.4. Cloning of 5' and 3' HAs into the pP{white-STAR} vector. After expected fragments were obtained, all positive colonies were sent to Sanger sequencing using universal T7 and SP6 primers along with sequencing primers and reverse and forward primers for each HA. Sequencing results revealed that one colony for each HA does not have any mutation. Therefore, we continued our strategy by digesting and ligating the 5' HA and 3' HA consecutively into the targeting vector pP{white-STAR}. First, the 5' HA and pP{white-STAR} vector were digested using *Kpn*I and *Avr*II (Figure 4.16). As three colonies gave the expected linearization pattern after *EcoR*I digestion, the successful 5' HA ligation to the targeting vector was confirmed (Figure 4.17). Then, this ligation product was digested with *Nhe*I and *Sac*II to clone the 3'HA into the vector. After performing the ligation reaction the products were transformed and plated on LB agar. Using the picked colonies the next day, cultures were started and obtained plasmids were double digested with *Spe*I-*Sma*I, *Kpn*I-*Avr*II, and *Nhe*I-*Sac*II to confirm the presence of

both the 5’ HA and the 3’ HA in the pP{white-STAR} targeting vector (Figure 4.18). Expected bands with lengths of 12 kb and 2300 bp for *Spe*I-*Sma*I digestion, 11 kb and 3253 bp for *Kpn*I-*Avr*II digestion, and 11 kb and 3385 bp for *Nhe*I-*Sac*II digestion confirmed the successful cloning of 5’ and 3’ HAs into the pP{white-STAR} targeting vector.

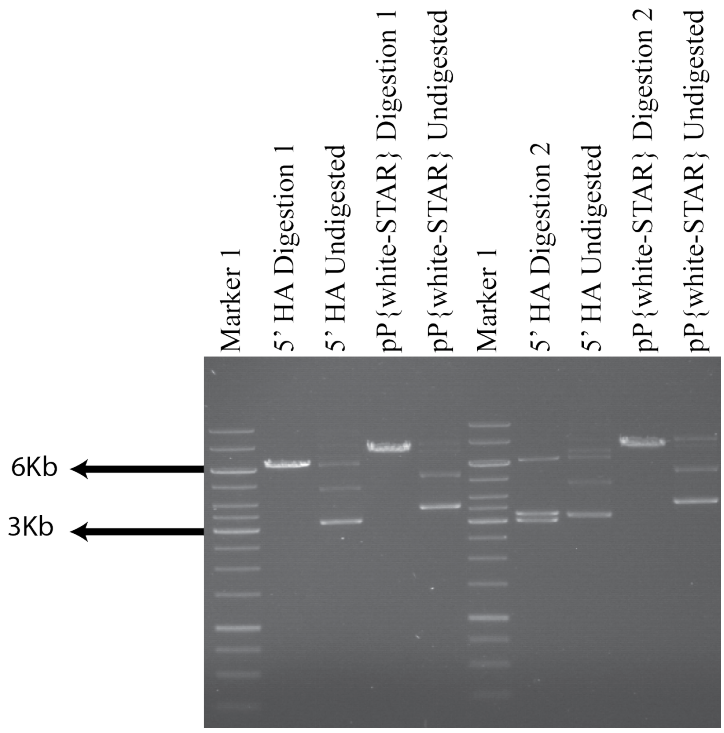

Figure 4.16. Analytic digestion of the 5’ HA and pP{white-STAR} vector using *Kpn*I (Digestion 1) and *Kpn*I-*Avr*II (Digestion 2). Marker 1 stands for 1kb DNA ladder (SM0311, Thermo Scientific). Both 5’ HA and pP{white-STAR} vector were first linearized with *Kpn*I only digestion and then expected fragments were obtained with the help of *Kpn*I-*Avr*II double digestion.

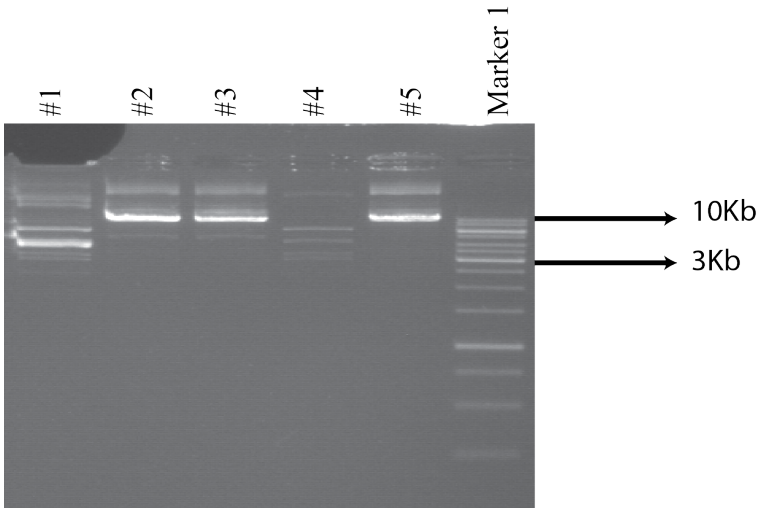

Figure 4.17. The confirmation of the presence of the 5'HA in pP{white- STAR} by *Eco*RI digestion. Marker 1 stands for 1kb DNA ladder (SM0311, Thermo Scientific). The presence of 5' HA in pP{white- STAR} was confirmed by observing the expected linearization pattern (#5).

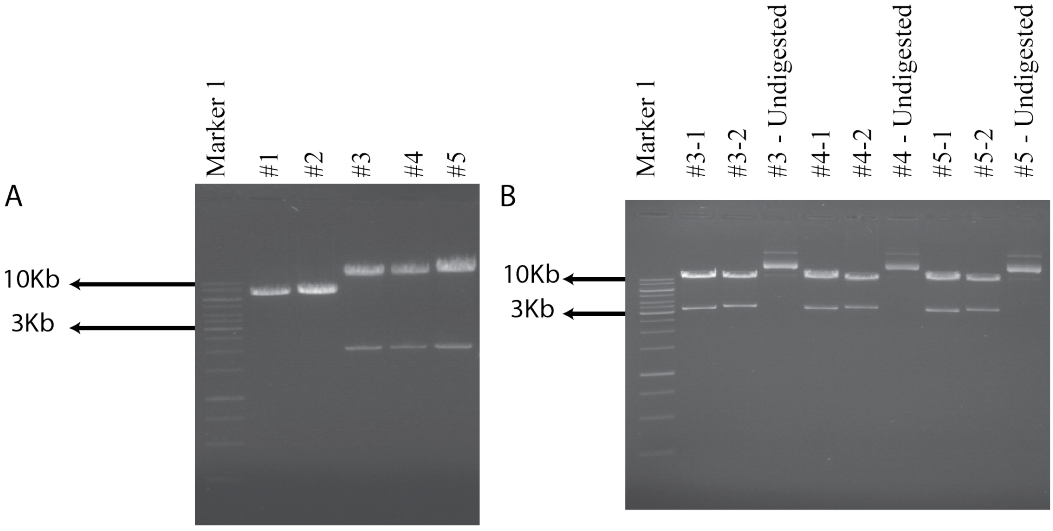

Figure 4.18. The confirmation of the presence of 5' and 3' HA in pP{white-STAR} using double digestion with *Spe*I-*Sma*I, *Kpn*I-*Avr*II and *Nhe*I-*Sac*II. *Spe*I-*Sma*I (A) together with *Kpn*I-*Avr*II (#3-1, #4-1 and #5-1) and *Nhe*I-*Sac*II (#3-2, #4-2 and #5-2) (B) revealed the presence of both 5'HA and 3'HA in pP{white- STAR}. Marker 1 stands for 1kb DNA ladder (SM0311, Thermo Scientific).

After confirming the correctness of the targeting construct for *CG4623*, the bacterial clone containing the targeting vector was sent to Genetic Services, Inc., USA for injection into fly embryos for site directed integration. For the landing site of the targeting

construct, *attP40*, which is on the second chromosome of *Drosophila melanogaster* genome, was selected to be able to track the mobilization of the element during future experiments and to differentiate it from the endogenous locus, which is on the third chromosome.

4.2.2. Generation of *CG4623* Knockout Flies

After obtaining two fly lines, *IMAGOCGL1* & *IMAGOCGL2*, carrying the targeting vector for *CG4623*, the eye colors of the progeny were observed. The presence of the red eye color confirmed that the construct was successfully integrated into the fly genome. However, interestingly only the female flies had red eyes, indicating that the targeting vector is located on the X chromosome and not on the 2nd chromosome. To confirm this observation, IMAGO transgenic lines were crossed with quadruple balancer lines. At the end of this balancing process, flies with the genotype of *sp/CyO; TM2/TM6B* were obtained confirming that the pP{white-STAR} was integrated on the X chromosome and not on the 2nd chromosome as expected. Homozygous flies for the IMAGO transgenic construct were obtained in the F2 progeny by crossing virgin IMAGO flies with male balancer *FM7a* flies (Figure 4.19).

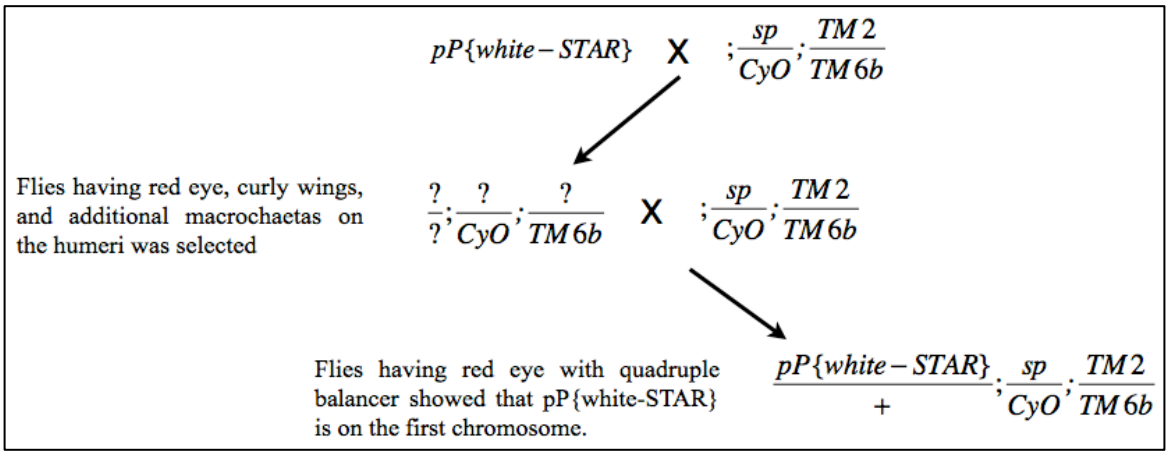

Figure 4.19. Mapping of the integrated pP{white-STAR} vector.

In order for homologous recombination to take place, male IMAGO flies were crossed with virgin female flies with the genotype of *hs-FLP, hs-I-Sce*I / *TM3*, *hs-hid* (Figure 4.20). Larvae from these crosses were heat-shocked for one hour at 38°C at the third and fourth days after crosses were set. Heat shocking activates the flippase and I-*Sce*I

enzymes; therefore, the integrated targeting construct should be mobilized and linearized with the help of these enzymes, respectively. The linearized fragment is expected to align with the region of the gene of interest, and the rare ends-out homologous recombination to occur in some of the cells. As the pP{white-STAR} vector contains the red eye marker, its excision from the genome with the help of flippase activity results in white eye color. The excised fragment recombines with the target gene in some of the cells resulting in red eye color. Therefore, we can analyze the success of homologous recombination by observing mosaic flies. As the marker is the eye color, the mosaicity in the eye can be used as a reporter of the occurrence of homologous recombination.

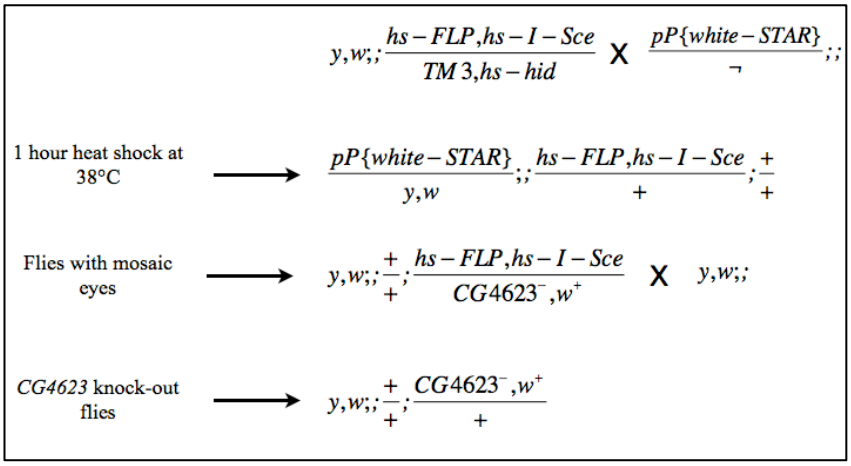

Figure 4.20. The cross scheme for the generation of *CG4623* knockout flies.

5. DISCUSSION

Perturbation of mitochondrial network dynamics and oxidative stress mechanisms are two of the major causes of neurodegenerative diseases. GDAP1 is one of the several known proteins having a role in the regulation of these mechanisms. It has been shown that GDAP1 is a key regulator of the mitochondrial fission machinery. Mutations in *GDAP1* are known to cause CMT that is the most common inherited peripheral neuropathy. In this study, we established the use of the IMAGO technique in our laboratory to generate a *Drosophila* model and study the pathophysiology of CMT. First, we determined that *CG4623* is the *Drosophila* homolog of *GDAP1* using the Flybase database. We, then, used the strategy to generate *CG4623* deficient fly lines by both RNAi and IMAGO approaches and also initiated the analyses to study the effects of the down-regulation of *CG4623*.

In the first part of the project, the expression of *CG4623* was down-regulated spatially using RNAi and its effects on mitochondrial morphology was analyzed. The methodology was established in our laboratory to analyze mitochondrial morphology focusing on the motor nerve bundles and eye imaginal discs, as these tissues are part of the peripheral nervous system of *Drosophila*. Using the GAL4-UAS binary system, double stranded RNA for part of *CG4623* mRNA and a GFP coding sequence fused to a mitochondrial import signal, both of which were found downstream of UAS elements, were expressed with various drivers. Preliminary data showed presence of elongated mitochondria in nerve bundles when the expression of *CG4623* was reduced with RNAi. On the other hand, we could not observe any significant difference between control and RNAi samples, when we analyzed the mitochondria in the eye imaginal discs. However, to obtain statistically significant results and confirm these findings these experiments should be repeated.

In the second part of the project, we initiated the use of an integrase-mediated approach for gene knockout (IMAGO) method to generate a CMT model. This method not only enables precise deletion of *CG4623,* but also the knock-in of wild type and mutated forms of human *GDAP1* into the fly genome. We have prepared the targeting construct and it was integrated into to the fly genome. We have tested the integration site of the target

vector by setting up crosses with balancer flies and found it to be integrated to the X chromosome. The IMAGO line was crossed further with the mobilization line to initiate homologous recombination and replace the *CG4623* gene with the red eye marker gene. Since recombinant flies could not be obtained yet, further steps include an increase in the number of crosses that are analyzed, and an optimization of the protocol for duration and temperature at which heat shock is induced to initiate mobilization and promote homologous recombination.

5.1. Down-regulation of *CG4623*

It is suggested that GDAP1 is the key regulator of mitochondrial fission. Its down-regulation in cell cultures results in more elongated mitochondria while its overexpression causes more circular ones. As it has been speculated, *GDAP1* mutations associated with CMT may result in the disease due to perturbation of mitochondrial network dynamics and oxidative stress, we wanted to analyze mitochondrial morphology in the flies upon down-regulation of the fly homolog, *CG4623*. For this purpose, ubiquitous, neuronal, and glial down-regulation were achieved in flies using RNAi with the help of the GAL4/UAS binary system. To analyze mitochondrial morphology together with the down regulation, we recombined the RNAi and mitoGFP alleles onto the same chromosome.

In order to confirm down-regulation of *CG4623*, we performed qRT-PCR experiments and showed that the mRNA level of *CG4623* was reduced to 12% in these flies. The effects of this decrease on mitochondrial morphology were analyzed in eye imaginal discs. The eye imaginal disc, which will be a part of the peripheral nervous system as developed adult eye in flies, was selected as a model since it is known that loss of GDAP1 function causes peripheral neuropathy. As another component of the peripheral nervous system, motor and sensory nerve bundles projecting from the ventral nerve cord were also analyzed in terms of mitochondrial morphology. The adult eye develops from the eye imaginal disc, an epithelial sheet of differentiated and undifferentiated cells. However, since eye imaginal disc is a highly compact and crowded structure compared to the motor and sensory nerve bundles originating from the ventral nerve cord, it was very difficult to visualize mitochondria as single entities and quantify them in its dense cellular environment.

The mitochondrial network dynamics has been investigated using immunohistochemistry and subsequent confocal microscopy. We analyzed the imaginal eyes discs of the larvae at which *CG4623* expression was down-regulated spatially in neuronal and glial tissues. When we compared the eye imaginal discs of the larvae of control and RNAi experiments, we did not observe any significant difference in terms of mitochondrial parameters such as elongation index. In these analyses, we used seven to eight eye imaginal discs for both control and RNAi experiments and the morphology index difference was not significant between them. A higher number of samples should be analyzed to reach significance in the compared parameters regarding mitochondrial dynamics.

In order to analyze this structure, we took maximum projections of the images of z-stacks from each experiment. Because of that mitochondria from different stacks might have been observed on top of each other and a single circular mitochondrion from different stages might have been analyzed as an elongated mitochondrion. On the other hand, if an elongated mitochondrion is placed in three different stacks we might have seen its parts from each stack as a different or circular mitochondrion, unless we take the maximum projections of the z-stacks. Furthermore, as mitochondria are not positioned in the same direction in three dimensions, it is impossible to analyze their morphology with precision unless three-dimensional reconstructions are analyzed in terms of their volume and surface area, for which no available imaging analysis tool exists to the best of our knowledge.

In this project, we used the Mitochondrial Morphology, a plug-in for ImageJ software, to analyze the images we obtain by confocal microscopy (Dagda *et al*., 2009). This macro analyzes several parameters such as perimeter and circularity of the binary images converted by auto-thresholding. It gives all of the quantifications with their averages. The effectiveness of this plug-in was compared to visual inspection and counting and similar results could not be obtained (Figure 5.1). At first, it was thought that the macro quantified mitochondrial morphology with little accuracy due to the density of the sample. However, it was possibly due to loss of the three dimensional information by taking the maximum projection of the z-stacks together and increasing the average size of mitochondria by merging GFP signals from different stacks.

A maximum projection of a nerve bundle image was used to test the efficiency of the macro used for image analysis. This image was selected since it allows individual identification of mitochondria. The macro is not considering a single pixel as a single circular mitochondrion since it could be a signal that is coming from a lower layer, an artifact or fragmented mitochondria that were not recycled through mitophagy. Instead, these were considered as a mitochondrion when there were at least two pixels next to each other producing continuous pixels. When the data was compared to that of counts performed manually, the plug-in gave only four mitochondria although we have determined the value to be 27. Therefore, the structure of the tissues is affecting the mitochondrial morphology analyses with this plug-in dramatically and it gives inconsistent results although it analyzes a more quantifiable image.

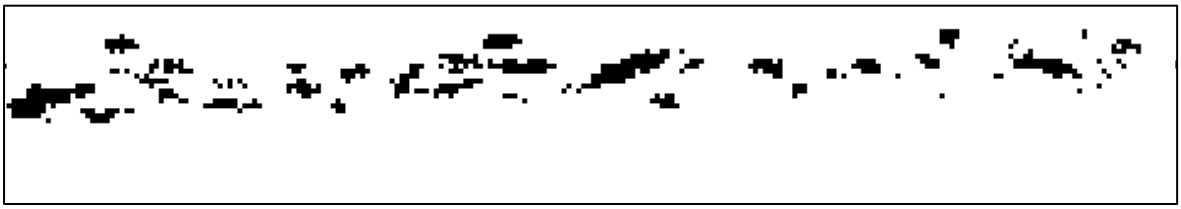

Figure 5.1. Analysis to count the mitochondria within a single nerve bundle.

Table 5.1 Analyses of the nerve bundle using Mitochondrial Morphology plug-in for ImageJ software.

Count	4
Total Area of Mitochondria	11.2568
Cellular Area	1009.9991
Mito Content	1.1145
Perimeter Mitochondria	38.4825
Circularity mitochondria	1.4912
Avg. Perimeter	9.6206
Avg. Area	2.8142
Avg. Circularity	0.3728
Area/Perimeter	0.2925
Area/Perimeter normalized to minor axis.	0.3148
Minor Axis	0.9291
Area/Perimeter normalized to circularity	0.7847

Although the eye imaginal disc is a part of the peripheral nervous system of the fly, it is not a good tissue to study mitochondrial morphology due to its dense structure and intricate organization. Therefore, in order to obtain quantifications with available computational tools, single neurons have to be visualized. For example, the giant fiber in the adult stage and nerve bundles originating from the ventral nerve cord although more difficult to dissect should be preferred as a model in future studies. It should also be noted that since CMT is a peripheral neuropathy that affects lower extremities compared to the proximal regions of the nervous system, neurons innervating muscles A2 and A7 can be used as models. The lengths of these neurons differ, making them good models to analyze the distance-dependent effect in this neuropathy. Similarly, mitochondrial network dynamics can be analyzed by *in vivo* live imaging of the giant fiber axon that is the longest neuron in flies. The giant fiber axon is long enough to allow visualization of not only fission and fusion events, but also the motility and movement of mitochondria. It is perceivable that defects in movement could also be caused by some of the *GDAP1* mutations observed in human.

5.2. IMAGO

The function of the fly homolog of *GDAP1,* CG4623, is not known yet as its name indicates. Bioinformatics analyses have revealed that it is the *Drosophila* homolog of *GDAP1* and GDAP1L1 (Marco *et al*., 2004). In order to understand whether *GDAP1* and *CG4623* are functional homologs, it should be knocked-out from the fly genome and be replaced with human *GDAP1* to see if the human protein rescues the possible phenotypes or not. For this purpose, homologous recombination is the best strategy for deleting the gene, since this technique generates a precise knockout compared to *P*-element excision. Therefore, we decided to knockout *CG4623* from the fly genome using the IMAGO method, which is based on classical ends-out homologous recombination technique.

The reason for choosing IMAGO instead of classical ends-out homologous recombination is because it allows the replacement of the marker gene with the coding sequence of any gene of interest, including wild type and mutant forms of *GDAP1,* using recombinase-mediated cassette exchange (RMCE). These repetitive replacements are possible due to the presence of two *attP* sites flanking the red eye marker (w^+) in the

targeting vector, pP{white-STAR}. Using IMAGO, it is not only possible to replace the red eye marker with the mutant and the wild type form of *GDAP1,* but also with a reporter gene such as mCherry or a GFP-fused form of *CG4623*. Therefore, with the help of immunohistochemistry the localization of CG4623 can be further analyzed. Furthermore, HA or FLAG tagged forms of CG4623 can be used to investigate the interaction partners of the protein. Hence, downstream and upstream factors in pathways that CG4623 have a role could be determined. In addition to these, a GAL4 driver line can be generated by using this technique. Thus, with the help of the GAL4/UAS binary system, any protein can be expressed where *CG4623* is expressed.

In order to replace *CG4623* with the red eye marker (w^+), we prepared the targeting vector containing 5' and 3' homology arms that flank the gene of interest. These 3 kb long homology arms were first amplified and subcloned into pGEM-T easy vector and sequenced to ensure that there were no mutations in these regions. Then these homology arms were consecutively cloned into the pP{white-STAR} backbone. The prepared construct was sent to Genetic Services, Inc, USA, for site-specific integration into the *Drosophila melanogaster* genome using *attP40* as the landing site, which corresponds to the second chromosome.

Drosophila melanogaster has four chromosome pairs, and *CG4623* is on the left arm of the third chromosome. We have chosen the second chromosome, which harbors *attP40*, as the landing site for the targeting vector. The third chromosome, on which *CG4623* is located, is not chosen as the target to avoid secondary mutations that may arise due to genetic manipulation on the chromosome itself. To eliminate any off-target effects when *CG4623* is knocked out, the chromosome previously carrying the targeting construct has to be isogenized with a wildtype chromosome. Isogenization will not be possible if the knock-out allele and the landing site are on the same chromosome. The aim of this methodology is to obtain flies that differ from wild type only for *CG4623* with no other mutations in different parts of the genome.

The fourth chromosome was not chosen as the landing site since it is very tiny and there are no balancer lines. Thus, a choice has been done between the X and the second chromosome. The second chromosome has been preferred instead of X, because of its

hemizygosity and also lack of lethal balancer lines that restricts keeping of the stock over time. When we received the flies, we have observed that not males but only the female flies had red eyes, which is the marker gene on our target vector. Therefore, we thought that our targeting construct might have integrated into the X chromosome. In order to understand on which chromosome our targeting construct was integrated, we had set crosses for mapping the location of the pP{white-STAR} with a quadruple balancer line. It was observed that our construct was on the X chromosome. Although site-specific integration has been opted for injection service, there is always a possibility of random integration into the genome as this vector includes *P*-element ends. However, this unexpected integration does not affect the progression of the project because it has not integrated into the third chromosome, where our gene of interest is located.

Crosses were set between our IMAGO flies and fly lines harboring heat shock inducible flippase and the rare cutter I-*Sce*I genes in their genome to mobilize the pP{white-STAR} vector and promote homologous recombination. It is known that only a linear DNA fragment could undergo homologous recombination in the nucleus and homologous recombination is a very rare event depending on the genomic site of the gene of interest and other factors. We expected to observe mosaic eyes with white and red patches in the progeny of the cross between flies having the targeting construct crossed with *hs-FLP, hs-I-SceI*. We have set 30 crosses in the scope of this thesis study and could not observe any mosaic flies so far. Therefore, the number of crosses has to be increased in order to be able to spot a mosaic-eyed fly among the progeny. In addition, the heat shock process may not be efficient enough to activate flippase and I-*Sce*I enzymes. If this was the case, this would results in an inability of the construct to flip out and be linearized. Since heat shock is the initiation point of flip-out and linearization, the flies can be exposed to heat shock at different time intervals. The date at which heat shock is performed can be changed to an earlier developmental period in larval stages, as well. It can be performed the day after crosses were set or it can be extended to three days instead of two days.

6. CONCLUSION

In this study, we initiated molecular studies to develop a *Drosophila melanogaster* model for CMT and established the methodology to analyze mitochondrial morphology in the peripheral nervous system of *Drosophila*. RNAi lines were utilized to reduce the expression of *CG4623* and its down-regulation was confirmed with qRT-PCR. Initial data revealed elongated mitochondria in these flies that confirm the suspected fission effects of the gene on the mitochondrial morphology. Generation of viable flies with *CG4623* down-regulation will allow further studies to be performed to unravel the function of the gene. In the second part of the study, recombinant flies have been produced that harbor the required construct to knockout the *CG4623* gene by homologous recombination. Initial crosses have not produced the knockout flies, yet, bringing the necessity of setting a high number of crosses to induce recombination using different experimental conditions. It will be possible to replace *CG4623* with human *GDAP1* and its mutant forms with the established techniques and fly lines generated in this study. This study is important since it has initiated the studies for generation of *Drosophila* as a model for genetic diseases in our country. With this model in our lab, it will be possible to confirm that *CG4623* is the functional homolog of *GDAP1* and study the effects of mutated versions of *GDAP1* on mitochondria. Chemicals that can be used as potential drugs for the treatment of CMT4A can be screened on these flies to treat the disease associated with elongated mitochondria morphology.

APPENDIX A: DATA OF THE MITOCHONDRIAL MORPHOLOGY ANALYSES USING IMAGEJ PLUG-IN

The elongation indices of mitochondrial morphology from each larva were measured for ubiquitous, pan-neuronal and pan-glial down-regulation of *CG4623* using ImageJ software. They are listed in Table A.1-A.3, respectively.

Table A.1. Individual elongation indices of ubiquitous down-regulation of *CG4623* and control larvae.

	L1	**L2**	**L3**	**L4**	**L5**	**L6**	**L7**
RNAi	0.12300	0.11889	0.33337	0.36771	0.15048	0.08666	0.10854
Control	0.09994	0.14866	0.11363	0.28399	0.12354	0.18165	0.12022

Table A.2. Average elongation index of ubiquitous down-regulation of *CG4623* and control larvae.

	Average	**Standard Deviation**	**p-value**
RNAi	0.184094198	0.115696287	0.5458
Control	0.153090876	0.063649116	

Table A.3. Individual elongation indices of pan-neuronal down-regulation of *CG4623* and control larvae.

	L1	**L2**	**L3**	**L4**	**L5**	**L6**	**L7**	**L8**	**L9**
RNAi	0.1134	0.1126	0.1564	0.0905	0.1967	0.2347	0.1196	0.1138	0.2149
Control	0.1044	0.1186	0.1373	0.0885	0.2327	0.0885	0.0877	0.1464	0.1024

Table A.4. Average elongation indices of pan-neuronal down-regulation and control larvae.

	Average	**Standard Deviation**	**p-Value**
RNAi	0.150272098	0.052589114	0.2591
Control	0.12295015	0.046355905	

Table A.5. Individual elongation indices of pan-glial down-regulation of *CG4623* and control larvae.

	L1	**L2**	**L3**	**L4**	**L5**	**L6**	**L7**	**L8**	**L9**
RNAi	0.107	0.060	0.063	0.214	0.091	0.066	0.081	0.110	0.084
Control	0.088	0.098	0.078	0.070	0.082	0.065	0.081	0.064	0.065

Table A.6. Average elongation indices of panglial down-regulation and control larvae.

	Average	**Standard Deviation**	**p-Value**
RNAi	0.097442659	0.047172649	0.2147
Control	0.076564526	0.011796982	

REFERENCES

Adams, M.D., S.E. Celniker, R.A. Holt, C.A. Evans, J.D. Gocayne, P.G. Amanatides, S.E. Scherer, P.W. Li, R.A. Hoskins, R.F. Galle *et al*. 2000, “The Genome Sequence of Drosophila melanogaster”, *Science*, Vol. 287, No. 5461, pp. 2185-2195.

Altschul, S. F., T. L. Madden, A. A. Schaffer, J. Zhang, Z. Zhang, W. Miller, and D. J. Lipman, 1997, "Gapped Blast and Psi-Blast: A New Generation of Protein Database Search Programs", *Nucleic Acids Research*, Vol.25, No. 17, pp. 3389-402.

Altschul, S. F., J. C. Wootton, E. M. Gertz, R. Agarwala, A. Morgulis, A. A. Schäffer, and Y. Yu, 2005, "Protein Database Searches Using Compositionally Adjusted Substitution Matrices", *the FEBS Journal,* Vol. 272, No 1, pp. 5101-5109.

Berman, S. B., F. J. Pineda, and J. M Hardwick, 2008, “Mitochondrial Fission and Fusion Dynamics: the Long and Short of It”, *Cell Death and Differentiation*, Vol. 15, No. 7, pp. 1147-1152.

Bhatheja, K. and J. Field, 2006, "Schwann Cells: Origins and Role in Axonal Maintenance and Regeneration", *The International Journal of Biochemistry and Cell Biology*, Vol. 38, No. 12, pp. 1995-9.

Board, P. G. and D. Menon, 2013, "Glutathione Transferases, Regulators of Cellular Metabolism and Physiology", *Biochimica et Biophysica Acta*, Vol. 1830, No. 5, pp. 3267-88.

Brand, A. H., and N. Perrimon, 1993, "Targeted Gene Expression as a Means of Altering Cell Fates and Generating Dominant Phenotypes", *Development*, Vol. 118, No. 2, pp. 401-15.

Bucci, C., O. Bakke, and C. Progida, 2012, "Charcot-Marie-Tooth Disease and Intracellular Traffic", *Progress in Neurobiology*, Vol. 99, No. 3, pp. 191-225.

Cassereau, J., A. Chevrollier, D. Bonneau, C. Verny, V. Procaccio, P. Reynier, and M. Ferre, 2011, "A Locus-Specific Database for Mutations in GDAP1 Allows Analysis of Genotype-Phenotype Correlations in Charcot-Marie-Tooth Diseases Type 4A and 2K", *Orphanet Journal of Rare Diseases,* Vol. 6, No. 87.

Chen, H. and D. C Chan., 2005, "Emerging Functions of Mammalian Mitochondrial Fusion and Fission" *Human Molecular Genetics*, Vol. 14, No. 2, pp. R283-289

Chen, H. and D. C. Chan, 2009, "Mitochondrial Dynamics − Fusion, Fission, Movement, and Mitophagy−in Neurodegenerative Diseases", *Human Molecular Genetics*, Volume 18, pp. 169-176.

Choi, C.M., S. Vilain, M. Langen, S. Van Kelst, N. De Geest, J. Yan, P. Verstreken, and B.A. Hassan, 2009, "Conditional Mutagenesis in Drosophila", *Science*, Vol. 324, No. 5923, p. 54.

Cuesta, A., L. Pedrola, T. Sevilla, J. Garcia-Planells, M. J. Chumillas, F. Mayordomo, E. LeGuern, I. Marin, J. J. Vilchey and F. Palau, 2002, "The Gene Encoding Ganglioside-induced Differentiation-associated Protein 1 is Mutated in Axonal Charcot-Marie-Tooth Type 4A Disease", *Nature Genetics*, Vol. 30, No. 1, pp. 22-25.

Curtiss, J. and M. Mlodzik, 2000, "Morphogenetic Furrow Initiation and Progression During Eye Development in Drosophila: The Roles of Decapentaplegic, Hedgehog and Eyes Absent", *Development*, Vol. 127, No. 6, pp. 1325-36.

Dietzl, G., D. Chen, F. Schnorrer, K. C. Su, Y. Barinova, M. Fellner, B. Gasser, K. Kinsey, S. Oppel, S. Scheiblauer *et al*., 2007, "A Genome-Wide Transgenic RNAi Library for Conditional Gene Inactivation in Drosophila", *Nature*, Vol. 448, No. 7150, pp. 151-6.

Duffy, J. B., 2002, "Gal4 System in Drosophila: A Fly Geneticist's Swiss Army Knife", *Genesis*, Vol. 34, No. 1-2, pp. 1-15.

Dyck, P. J., P. Chance, R. Lebo, J.A. Carney and P.K. Thomas, 1993, *Peripheral Neuropathy*, 3rd edition, W.B. Saunders, Philadelphia.

Garbay, B., A. M. Heape, F. Sargueil, and C. Cassagne, 2000, "Myelin Synthesis in the Peripheral Nervous System", *Progressive Neurobiology*, Vol. 61, No 3, pp 267-304.

Harding, A. E., and P. K. Thomas, 1980, "Genetic Aspects of Hereditary Motor and Sensory Neuropathy (Types I and II)", *Journal of Medical Genetics*, Vol. 17, No. 5, pp. 329-336.

Hsieh, S. Y., H. C. Kuo, C. C. Chu, K. P. Lin and C. C. Huang, 2004, "Charcot-Marie-Tooth Disease Type 1A: A Clinical, Electrophysiological, Pathological, and Genetic Study", *Chang Gung Medical Journal*, Vol. 27, No. 4, pp. 300-306.

Jessen, K. R., 2004, "Glial Cells", *The International Journal of Biochemistry and Cell Biology*, Vol. 36, No. 10, pp. 1861-1867.

Kaçmaz, G., 2013, *Characterization of a Novel R7-Specific Gene in the Drosophila Visual System*, M.Sc. Thesis, Boğaziçi University.

Lupski, J. R., R. M. de Oca-Luna, S. Slaugenhaupt, L. Pentao, V. Guzzetta, B. J. Trask, O. Saucedo-Cardenas, D. F. Barker, J. M. Killian, C. A. Garcia *et al*., 1991, "DNA Duplication Associated with Charcot-Marie-Tooth Disease Type 1A", *Cell*, Vol. 66, No. 2, pp. 219-232.

Marco, A., A. Cuesta, L. Pedrola, F. Palau and I. Marin, 2004, "Evolutionary and Structural Analyses of GDAP1, Involved in Charcot-Marie-Tooth Disease, Characterize a Novel Class of Glutathione Transferase-Related Genes", *Molecular Biology of Evolution*, Vol. 21, No. 1, pp. 176-187.

Nelis, E., C. Van Broeckhoven, P. De Jonghe, A. Lofgren, A. Vandenberghe, P. Latour, E. Le Guern, A. Brice, M. L. Mostacciuolo, F. Schiavon *et al*., 1996, "Estimation of the Mutation Frequencies in Charcot-Marie-Tooth Disease Type 1 and Hereditary Neuropathy with Liability to Pressure Palsies: A European Collaborative Study", *European Journal of Human Genetics*, Vol. 4, No. 1, pp. 25-33.

Niemann, A., M. Ruegg, V. La Padula, A. Schenone and U. Suter, 2005, "Ganglioside-induced Differentiation-associated Protein 1 is a Regulator of the Mitochondrial Network: New Implications for Charcot-Marie-Tooth Disease". *Journal of Cell Biology*, Vol. 170, No. 7, pp. 1067-1078.

Noack, R., S. Frede, P. Albrecht, N. Henke, A. Pfeiffer, K. Knoll, T. Dehmel, G. Meyer zu Horste, M. Stettner, B. C. Kieseler *et al*., 2012, "Charcot-Marie-Tooth Disease CMT4A: GDAP1 Increases Cellular Glutathione and the Mitochondrial Membrane Potential", *Human Molecular Genetics*, Vol. 21, No. 1, pp. 150-162.

Pandey, U. B., and C. D. Nichols, 2011, "Human Disease Models in Drosophila Melanogaster and the Role of the Fly in Therapeutic Drug Discovery", *Pharmacological Reviews*, Vol. 63, No. 2, pp. 411-436.

Pedrola, L., A. Espert, T. Valdes-Sanchez, M. Sanchez-Piris, E. E. Sirkowski, S. S. Scherer, I. Farinasc and F. Palaua, 2008, "Cell Expression of GDAP1 in the Nervous System and Pathogenesis of Charcot-Marie-Tooth type 4A disease", *Journal of Cellular and Molecular Medicine*, Vol. 12, No. 2, pp. 679-689.

Pla-Martin, D., C. B. Rueda, A. Estela, M. Sanchez-Piris, P. Gonzalez-Sanchez, J. Traba, S. de la Fuente, L. Scorrano, J. Renau-Piqueras, J. Alvarez *et al*., "Silencing of the Charcot-Marie-Tooth Disease-Associated Gene Gdap1 Induces Abnormal Mitochondrial Distribution and Affects Ca^{2+} Homeostasis by Reducing Store-Operated Ca^{2+} Entry", *Neurobiology of Disease*, Vol. 55, No. 1, pp. 140-151.

Rong, Y. S., and K. G. Golic, 2003, "The Homologous Chromosome is an Effective Template for the Repair of Mitotic DNA Double-Strand Breaks in Drosophila", *Genetics*, Vol. 165, No. 4, pp. 1831-1842.

Scherer, S. S. and E. J. Arroya, 2005, “Schwann Cells”, *Encyclopedia of Life Sciences*, pp. 1-9.

Shield, A. J., T. P. Murray and P. G. Board, 2006, “Functional Characterisation of Ganglioside-induced Differentiation-associated Protein 1 as a Glutathione Transferase”, *Biochemical and Biophysical Research Communications*, Vol. 347, No. 4, pp. 859-866.

Shir Y. and Z. Seltzer, 1990, “A-fibers Mediate Mechanical Hyperesthesia and Allodynia and C-fibers Mediate Thermal Hyperalgesia in a New Model of Causalgiform Pain Disorders in Rats”, *Neuroscience Letters*, Vol. 115, No. 1, pp. 62-67.

Siskind, C. E., S. Panchal, C. O. Smith, S. M. Feely, J. C. Dalton, A. B. Schindler, and K. M. Krajewski, 2013, "A Review of Genetic Counseling for Charcot Marie Tooth Disease (CMT)", *Journal of Genetic Counseling*, Vol. 22, No. 4, pp. 422-36.

Skre, H., 1974, "Genetic and Clinical Aspects of Charcot-Marie-Tooth's Disease", *Clinical Genetics*, Vol. 6, No. 2, pp. 98-118.

Vallat, J. M., S. Mathis, and B. Funalot, 2013, "The Various Charcot-Marie-Tooth Diseases", *Current Opinion in Neurology*, Vol. 26, No. 5, pp. 473-480.

Wagner, K. M., M. Ruegg, A. Niemann, and U. Suter, 2009, "Targeting and Function of the Mitochondrial Fission Factor GDAP1 are Dependent on Its Tail-Anchor", *PLoS One*, Vol. 4, No. 4, pp. e5160.

Zuchner, S., and J. M. Vance, 2006, "Mechanisms of Disease: a Molecular Genetic Update on Hereditary Axonal Neuropathies", *Nature Clinical Practice Neurology*, Vol. 2, No. 1, pp. 45-53.